UNIVERSITÀ DEGLI STUDI DI MILANO

Department of Biomedical Sciences for Health

PhD course in Experimental Medicine and Medical Biotechnologies

XXX cycle

ROLE OF FERROPORTIN-MEDIATED

IRON RELEASE FROM MACROPHAGES

IN TISSUE HOMEOSTASIS AND REPAIR

Ph.D. thesis of:

Paolo BURATTI

Matr. n. **R10900**

Supervisor: Prof.ssa **Stefania RECALCATI**

Co-Supervisor: Prof. **Gaetano CAIRO**

Coordinator: Prof. **Massimo LOCATI**

Academic year 2017 – 2018

TABLE OF CONTENTS

1. ABSTRACT

Macrophages are essential in the inflammatory response and also have a critical function in body iron homeostasis. Moreover, it is known that iron metabolism is important in the context of inflammation. Indeed, it has been demonstrated that, in line with their functions, distinct macrophage populations, such as M1 and M2 polarized cells, differ in the expression of genes involved in iron homeostasis as well as in the expression of immunoregulatory genes. The functional significance of these differencies are not completely understood: we hypotized that iron released by M2 macrophages could promote cell proliferation and extracellular matrix deposition in the resolution phase of inflammation. Moreover, in line with the increasing awareness that macrophages have an important trophic role in addition to their immunological function, macrophages may play a role of "local iron redistributors" in tissues, where they would manage iron availability for neighbouring cells. Therefore, the major aim of this project was to exploit a mouse model of impaired iron release from macrophages, caused by deletion of Ferroportin (Fpn), to understand the functions of macrophage iron in two situations of tissue repair: cutaneous wound healing and liver fibrosis.

The characterization of mice with loss of macrophage Fpn showed that they are affected by transient alopecia caused by impaired hair follicle growth. The local impairment of iron distribution due to macrophage Fpn inactivation was accompanied by cellular iron deprivation and decreased proliferation in adjacent epithelial cells. By exposing mice to an iron-restricted diet we concluded that hair loss was not related to hypoferremia/anemia. Taken together, these results suggest that iron retention in resident macrophages has detrimental effects on tissue homeostasis by inhibiting the proliferation of hair follicle cells.

We observed a considerable delay in the closure of excisional skin wounds of Fpn$^{fl/fl}$Lys$^{Cre/-}$ mice compared to controls, with defective granulation tissue formation and diminished fibroplasia. Moreover, the development of both lymphatic and blood vascular network was impaired. Conversely, inactivation of Fpn in macrophages had no impact on inflammatory processes accompanying wound healing, such as production of inflammatory molecules, content of leukocyte subsets and macrophage polarization. Altogether, these results indicate that, though it does not interfere with immune cells recruitment and local activation, Fpn deletion in macrophages impairs blood vessels formation and stromal cells proliferation, leading to delayed skin repair.

Fpn inactivation in macrophages had no impact on inflammation, steatosis and fibrosis associated with exposition to the MCD diet, a model of non-alcoholic steatohepatitis. Levels of inflammatory and fibrogenic markers did not show significant differences between Fpn$^{fl/fl}$Lys$^{Cre/-}$ mice and controls. Interestingly, the levels of transaminases were significantly lower in mice with Fpn inactivation in macrophages, suggesting a different susceptibility to liver damage. These data suggest that, in this model, Fpn deletion in macrophages does not affect the inflammatory response to liver damage and fibrogenesis. The different susceptibility to liver damage and the different results we observed in the cutaneous wound healing and in the process of hepatic fibrosis should be further explored, perhaps using another model of fibrosis.

In conclusion, the results reported in this thesis indicate that the macrophage trophic function in skin homeostasis and healing is iron and Fpn-dependent.

2. INTRODUCTION

2.1 The importance of iron homeostasis

Iron is a key element for many physiological processes in most organisms, from bacteria to mammals: it is incorporated in proteins performing key functions, such as oxygen transport and storage (eg hemoglobin and myoglobin), electron transfer (eg cytochromes) and DNA synthesis [4]. However, an excess of "free" iron is dangerous since it could lead to the formation of Reactive Oxygen Species (ROS), capable of damaging biological molecules and hence leading to cell death and tissue injury [5]. Disorders in iron homeostasis can lead to either iron deficiency or iron overload and contribute to several medical conditions, such as anemia and hemochromatosis.

Control of iron levels is also fundamental for the outcome of the competition over iron between the host and the invading pathogens[6]. Since iron is a fundamental growth factor for most parasites and bacteria, these microorganisms have developed several mechanisms for acquiring iron in low-iron environments. These processes include: the secretion of molecules that bind free iron with very high affinity (siderophores), the absorption of heme released from red blood cells after hemolysis and the ability to obtain iron from host iron-binding proteins (such as hemoglobin, transferrin and lactoferrin) [6,7]. Conversely, given the important role of iron for pathogen virulence, it is not surprising that the host has developed various mechanisms to control iron availability.

Therefore, iron homeostasis is strictly regulated and appropriate iron levels are maintained thanks to a complex network of proteins that co-ordinately regulate absorption, storage, recycling and use of iron both at systemic and cellular levels [8].

2.1.1 Systemic iron metabolism

On average, an adult human body contains 3–5 g of iron (50 mg/kg). Approximately 60% (2500 mg) of the total body iron content is found in circulating hemoglobin, and most of the rest is represented by storage iron distributed throughout various body tissues. Only about 20 % of the daily iron requirement comes from diet; almost 80% comes from the recovery of the metal from senescent red blood cells by macrophages of the reticuloendothelial system in the spleen red pulp and liver (Kupffer cells). These specialized phagocytes, which differentiate and develop via a process dependent on the SPI-C transcription factor [9], process old and/or defective erythrocytes and return hemoglobin-derived iron to the circulation for a new utilization [10]. Iron absorption takes place in the proximal small intestine, near the gastro-duodenal junction; here, non-heme iron is absorbed principally through the activity of the Divalent Metal Transporter 1 (DMT1), which transports the metal, in its ferrous form (Fe^{2+}), from the intestinal lumen into the cytosol of the enterocytes (Figure 1); absorption of heme iron is quantitatively more important but less characterized at the molecular level. Once internalized in the duodenal
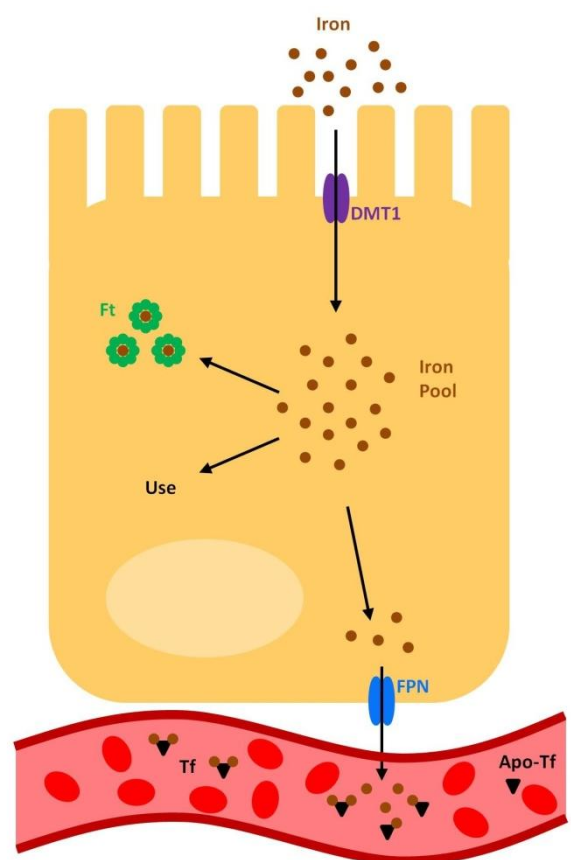

Figure 1. Iron absorption by duodenal enterocytes.

In duodenum iron is absorbed from diet via DMT1. Then is stored by Ft, used or released in the circulation via Fpn. In the bloodstream, iron is bound to serum protein Tf.

cell, iron can be stored by the iron storage protein ferritin (Ft) [11] or exported into plasma by ferroportin 1(Fpn), the only known mammalian non-heme iron exporter [12]. In the blood stream, iron is bound and safely carried to the various tissues by serum Tf (Figure 1). The Tf saturation by iron varies on a diurnal cycle and rapidly responds to local stimuli: it is higher in the portal circulation and lower in plasma leaving the erythroid bone marrow, where most of the iron is used by erythroid precursors cells. Under physiological conditions, Tf is partially saturated (around 30%) and can bind excess iron entering the circulation, thus protecting against iron toxicity.

The liver derived peptide hepcidin (HAMP) is the main regulator of systemic iron metabolism: it binds Fpn and induces its internalization and degradation [13]. By so doing, it plays a fundamental role in modulating the release of iron from duodenal enterocytes, spleen macrophages and hepatocytes, negatively modulating iron absorption from the diet, recycling from macrophages and also release from the liver [13], as hepatocytes serve as major depot for iron storage (Figure 2). At the systemic level, this mechanism results in a decrease in both plasma iron concentration and Tf
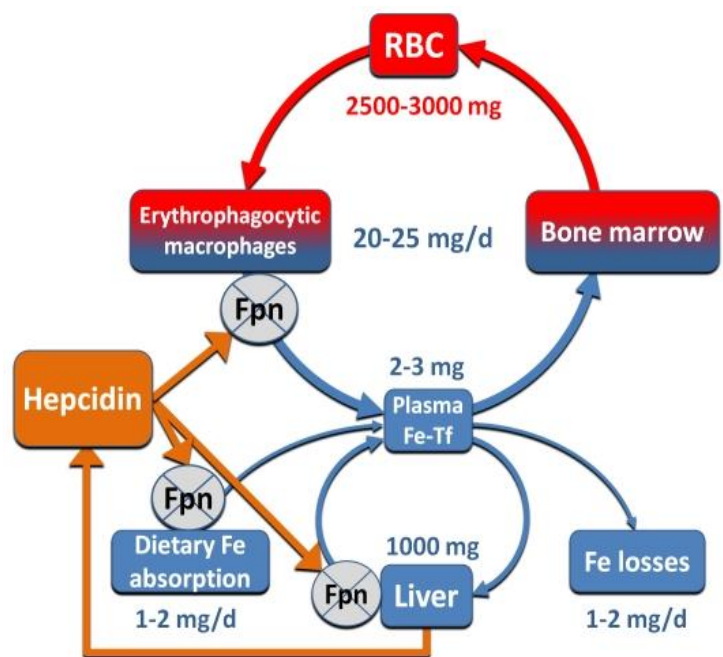

Figure 2.HAMP interaction with Fpn controls iron flux through plasma.

HAMP negatively modulates iron absorption from the diet, recycling from reticuloendothelial cells and release from liver storages [2]

saturation. HAMP expression is regulated by a variety of different signals; in particular, it is induced by iron stores and inflammatory stimuli [14]. In fact, HAMP is an acute-phase protein [15] and represents the mayor response of host iron metabolism upon microbial invasion and inflammation. It has been shown that interleukin 6 (IL-6), one of the most important pro-inflammatory cytokines involved in the acute phase response, promotes HAMP expression [16] thus blocking Fpn-dependent iron release and leading to hypoferremia and low Tf saturation. Of course, this restricted iron availability affects also erythroid progenitor cells, and prolonged hypoferremia may limit hemoglobin synthesis and cause the so-called anemia of chronic disease (ACD) [4,17].

2.1.2 Cellular iron metabolism

Cells that require iron express Transferrin Receptor 1 (TfR1) at the cell surface and, upon binding, the complex of TfR1 and iron-loaded Tf is internalized through a process of clathrin-mediated endocytosis [18] (Figure 3). Inside the cell, the endosome containing the internalized
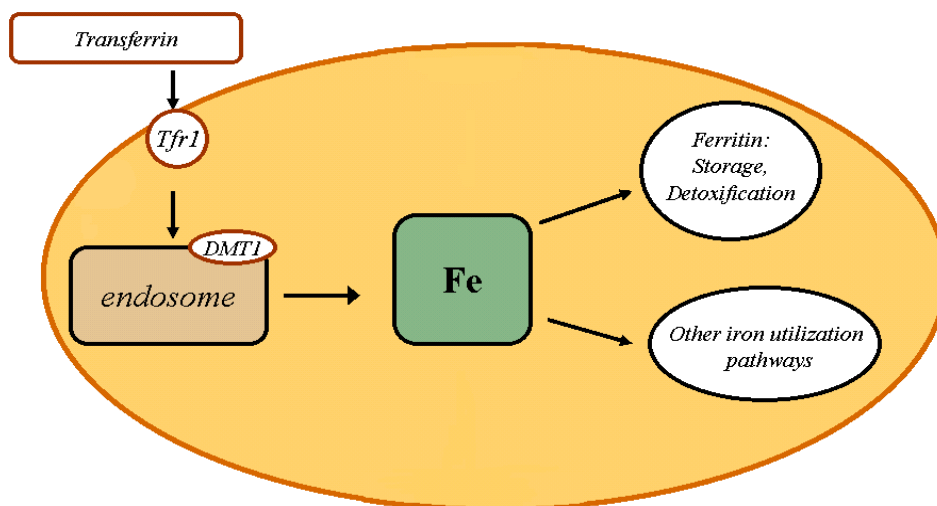

Figure 3. Iron entrance in the cell.
Tf interaction with Tfr1 causes the endocytosis of the protein complex and the release of iron in the cytosol. Iron can then be stored in Ft or used for the needs of the cell.

complex is acidified to a pH of about 5.5 by a vacuolar H^+-ATPase (V-ATPase). This acidification process produces conformational changes in the Tf-TfR1 complex with consequent release of iron, which is then transported to the cytosol by DMT1. At acidic pH, apo-transferrin (iron-free Tf) remains bound to TfR1 and the complex is recycled back to the cell surface. At the pH of the plasma, apo-transferrin dissociates from TfR1 and the receptor is ready for a new cycle of iron uptake [19]. Inside the cell, iron can be utilized for the metabolic needs of the cell itself, released through Fpn or stored for future necessities. In the last case, to avoid the intrinsic redox activity of the metal, the iron ions are sequestered by Ft, an heteropolymeric protein composed of 24 subunits assembled to form a spherical structure with an inner cavity in which iron is stored safely [20]. Therefore, Ft represents both a storage protein and an antioxidant factor. Fpn is a transmembrane protein that acts as an iron exporter, exporting iron out of cells. Fpn transports iron in its ferrous form, but an efficient iron export requires the activity of the oxidases ceruloplasmin (circulating) and hephaestin (membrane-bound, mainly expressed in the duodenum), which oxidize the metal to its ferric form that is accepted by Tf. Fpn structure has not yet been elucidated because there are no close structurally characterized homologs. The best-supported Fpn model has 12 transmembrane segments with both termini located intracellularly [21]. The crystal structure of a putative bacterial homolog of Fpn suggests that the protein is made of two lobes separated by a cytosolic loop [22]. The central cavity between the two lobes contains the iron-binding site and it can be either facing the cytosol or open to the extracellular space, depending on the spatial disposition of the two lobes. Transition between these two conformations could explain the iron export activity of Fpn.

The modulation of Fpn expression is complex and involves transcriptional, translational and post-translational mechanisms. The promoter of the Fpn gene contains hypoxia-response elements (HREs), targets of hypoxia Inducible Factors (HIFs), as shown by the HIF2alpha-dependent increase in Fpn transcription during hypoxia and iron deficiency [23]. On the contrary, inflammation decreases transcription of Fpn, though this mechanism is only partially characterized. LPS causes a downregulation of duodenal Fpn [24] and the Mycoplasma-derived molecule FSL1 reduces splenic and liver levels of Fpn mRNA [25]. At the translational level, iron itself modulates Fpn expression: in fact, Fpn mRNA contains a 5' iron response element (IRE), which under conditions of iron deficiency is bound by iron regulatory proteins (IRPs), thus resulting in translational repression [26]. Conversely, when iron is abundant IRPs binding activity is inhibited, thereby leading to active Fpn mRNA translation. IRPs are the major regulators of intracellular iron homeostasis, as they control also the translation of Ft and the stability of TfR1 mRNA. In addition, the activity of the transporter is predominantly governed post-translationally by HAMP: its binding to Fpn results in endocytosis and proteolysis of the exporter, predominantly in lysosomes [13]. Although the structural details of the HAMP-Fpn interaction are not fully understood, we now know that Fpn, as other receptors that undergo ligand-induced endocytosis, goes through a conformational change, followed by covalent modifications of its cytoplasmic segment. In addition, the interaction with HAMP causes ubiquitination of multiple lysine residues in the cytoplasmic loop connecting the two lobes of Fpn [27]. The details of this mechanism remain to be elucidated.

2.2 Macrophage iron metabolism

Resident macrophages are constitutively present in organs, in the absence of inflammation, and perform trophic and homeostatic functions: they remove apoptotic cells and serve as sentinels of injury and infection. Macrophages also play a critical role in body iron homeostasis: splenic reticuloendothelial macrophages recover iron from senescent erythrocytes and release it back to circulation. Macrophages play an essential role in the inflammatory response. In the site of inflammation are present recruited macrophages originated from peripheral blood monocytes, as well as resident macrophages, and both populations reveal a great heterogeneity of phenotypes and specialization: macrophages can acquire cytotoxic and antimicrobial activities i.e. classic pro-inflammatory (M1) macrophages, but also initiate repair and resolve inflammation, defined as alternative polarized (M2) macrophages [28].It is known that iron metabolism is important in the context of inflammation and in line with their different functions in homeostatic and inflammatory conditions, different macrophage populations differ in the expression of genes involved in iron homeostasis [29,30] as well as in the expression of immunoregulatory genes [31]. In particular, pro-inflammatory M1 macrophages show lower expression of Fpn and the consequent iron retention correlates with high expression levels of Ft [29] (Figure 4). On the contrary, alternative polarized M2 macrophages, involved in debris scavenging, angiogenesis and connective tissue remodelling, show higher expression of Fpn compared to M1 cells [29] (Figure 4): this sustains the propensity of M2 macrophages to actively export iron into the microenvironment [30,32]. These cells also show an increased expression of heme oxygenase (HO-1), which catalyzes the oxidative degradation of heme, endowed with pro-oxidant
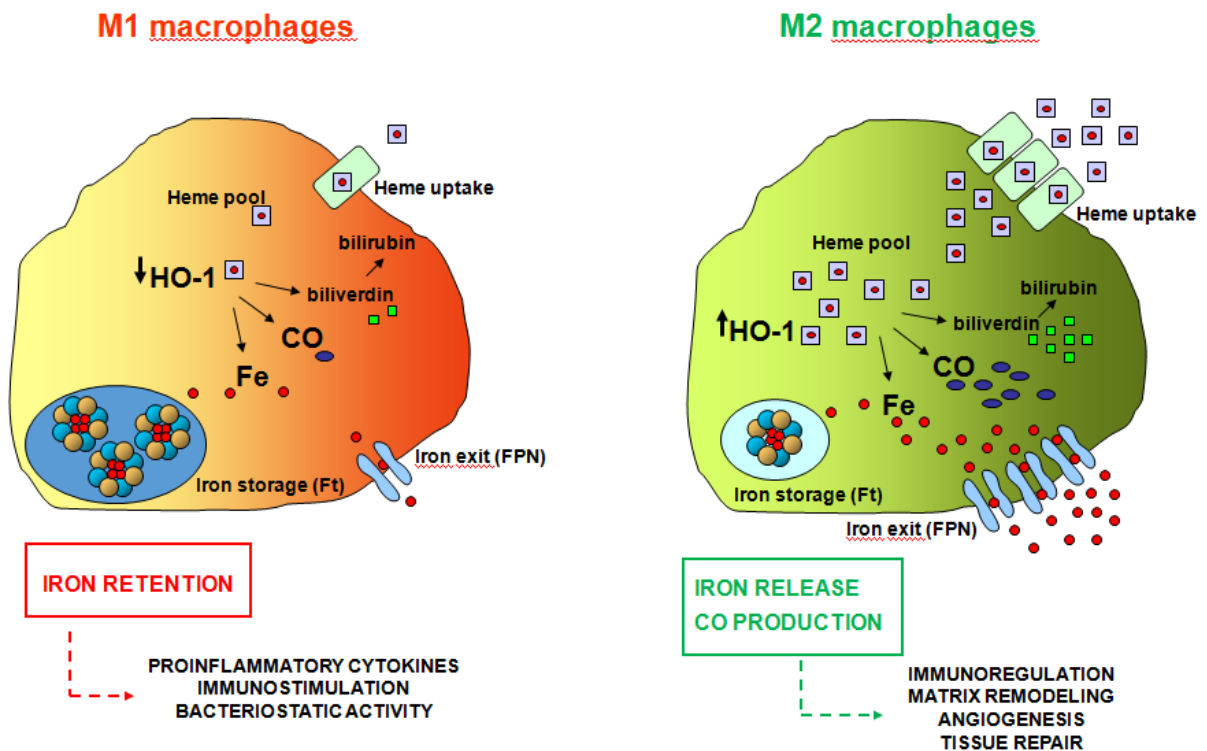
Figure 4. Macrophage polarization affects the expression of genes of iron homeostasis.
M1 macrophages are characterized by high Ft and low Fpn expression which sustains their inclination to store iron and deplete the microenvironment. On the contrary, M2 macrophages are characterized by low Ft and high Fpn, scavenger receptors and HO-1, which mediate efficient iron uptake and recirculation.

and pro-inflammatory activity. Heme catabolism produces iron, biliverdin, subsequently converted into bilirubin, possessing anti-inflammatory and anti-oxidant properties, and CO, which promotes vasodilatation and angiogenesis [30].

Moreover, a study [33] showed that M2 macrophages are characterized by improved expression of the Hb scavenger receptor CD163, increased heme uptake, heme-degradation and export of heme-derived iron. The greater availability of heme and non-heme iron in M2 macrophages cooperates with the high Fpn expression to increase ferrous iron export into the surrounding microenvironment (Figure 4).

The functional significance of these activities are not completely understood, it is reasonable to assume that iron released by M2

macrophages could be available for adjacent cells, such as fibroblasts, and promote proliferation and extracellular matrix (ECM) deposition. The latter function is in line with the iron-dependency of the prolyl hydroxylases required for collagen biosynthesis [34,35]. Moreover, heme scavenging could be a relevant mechanism to prevent the pro-oxidant and proinflammatory activities of this molecule, derived from the hemolysis that accompanies inflammation [36], while producing CO, with its anti-inflammatory and angiogenetic properties. Since inflammation is a dynamic process, it is also plausible that in the late phases of inflammation M2 macrophages release the iron previously accumulated under proinflammatory conditions, thus contributing to inflammation resolution.

2.3 Macrophages in skin homeostasis and tissue repair

In the skin, resident macrophages play an important role both in tissue homeostasis and in repair from injury [37-39]. Under physiological conditions, macrophages support parenchymal cells with trophic signals and nutrients and are critical regulators of hair follicle growth [40]: perifollicular macrophages stimulate hair follicle stem cells to enter in the growth phase (anagen) [41]. In pathological conditions, selective ablation of macrophages impairs various phases in the wound healing process [42]. Cutaneous wound healing is a dynamic process involving the differentiation, migration, proliferation, and apoptosis of various cell types, and is a very useful model to study macrophage differentiation and heterogeneity. Normal cutaneous wound repair is characterized by three major stages: the inflammatory, proliferative, and remodelling phases [3].

During the inflammatory phase, haemostasis represents the immediate response to injury and prevents blood loss at the wound site. Vascular injury causes a local activation of the innate immune system, resulting in an influx of inflammatory cells (Figure 5) attracted to the site of injury by cytokines, including transforming growth factor β (TGF-β) and platelet-derived growth factor (PDGF) [43,44]. Infiltrating neutrophils remove foreign corps from the wound area and are then extruded with the eschar or phagocytized by macrophages. In response to specific chemokines, monocytes infiltrate the wound area too and differentiate into
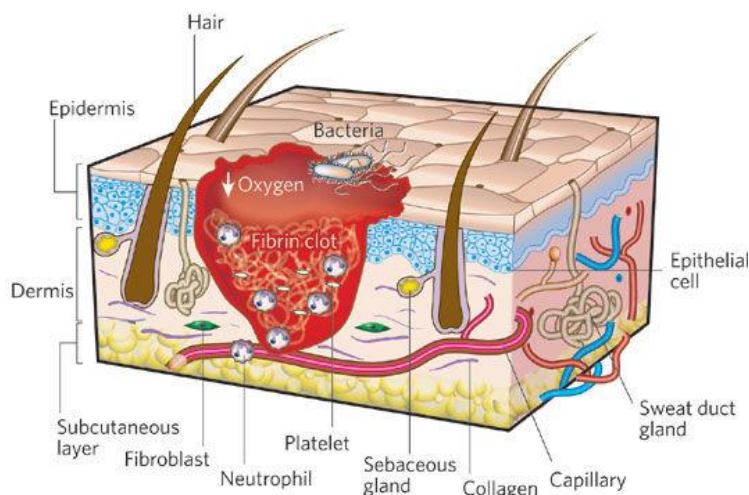
Figure 5. Stages of wound repair: inflammation.
Platelets facilitate haemostasis and secrete several mediators that attract and activate neutrophils and monocities (modified from [3]).

macrophages [45]. In this phase, the recruited and resident macrophage populations proliferate and undergo a classic pro-inflammatory M1 polarization, characterized by the production of oxygen radicals and pro-inflammatory cytokines and phagocytosis of foreign organisms. They also release TGF-β, PDGF and vascular endothelial growth factor (VEGF), thus stimulating the movement of fibroblasts and epithelial cells into the wound [37,38]. The inflammatory response is an essential component of the wound healing process: it is decisive to protect the body from foreign microorganisms and many of the cytokines and growth factors released during this process support the ensuing tissue repair. However, an

excessive inflammatory response or the presence of a chronic insult may lead to fibrosis and scar formation.

The proliferative phase is characterized by re-epithelialization of the epidermis, repair of the dermal layer and neo angiogenesis (Figure 6).
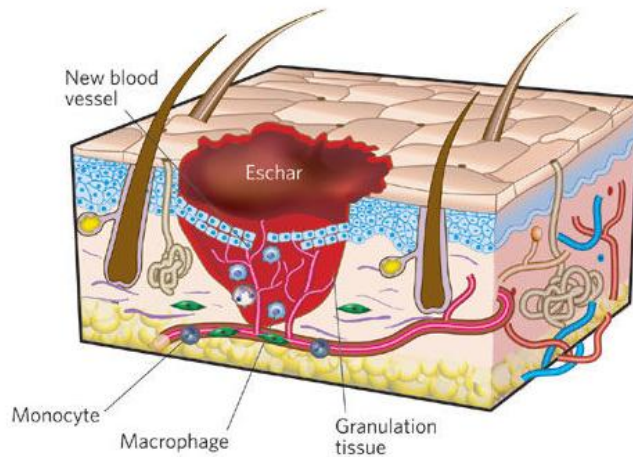

Figure 6. Stages of wound repair: proliferation.
Under the eschar, macrophages and fibroblasts invade the wound stimulating the formation of new blood vessels. All these events form the granulation tissue, the precursor of new stroma (modified from [3]).

The dermal wound space is refilled by invading and proliferating fibroblasts that separate the eschar from viable tissue. These fibroblasts synthesize and secrete extracellular matrix (ECM) that facilitates cell adhesion, migration and proliferation of other cells[46] and also release growth factors, such as TGF-β [47]. New stroma, also called granulation tissue, begins to occupy the wound area: macrophages and fibroblasts infiltrate the lesion space and new blood vessels form [43]. In this phase the macrophage populations show a M1 to M2 switch and alternative polarized macrophages, oriented to tissue repair and remodelling, predominate [37,48]. Macrophages represent a continuous source of growth factors (such as VEGF), so the M1 to M2 switch is essential for the healing process [38].

During the remodelling (or maturation) phase all the processes activated after injury come to an end : most of the endothelial cells, macrophages and fibroblasts undergo apoptosis or leave the wound site (Figure 7). Wound fibroblasts at this stage tend to adopt a contractile myofibroblast

phenotype [49,50] characterized by large bunches of actin microfilaments and cell-matrix and cell-cell linkages.
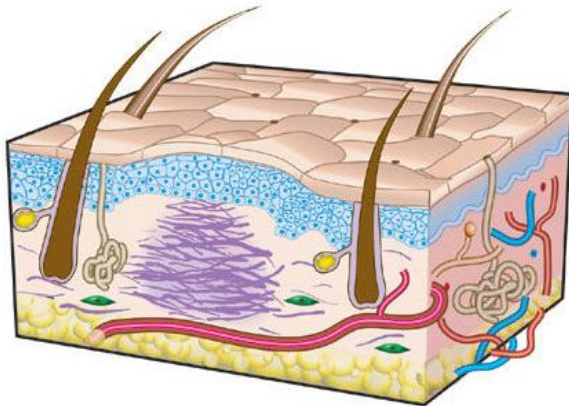

Figure 7. Stages of wound repair: maturation.
The shift of fibroblast to myofibroblast phenotype and the replacement of collagen type III with type I result in the contraction of the wound and new tissue formation (modified from [3]).

The maturation of the wound site, following deposition of ECM, changes the properties of the tissue: this involves the degradation and replacement of collagen type III with collagen I [3,44]. Collagen remodelling during the transition from granulation tissue to scar is mediated by several proteolytic enzymes called matrix metalloproteinases, secreted by macrophages, endothelial cells and fibroblasts. Together, these transformations result in the contraction of the wound and the arrangement of new tissue.

A tight control of iron metabolism is needed for appropriate skin wound healing. Previous evidence showed that excess iron, both in macrophages and in the extracellular environment, has a negative effect on tissue repair [51]. However, it is also plausible that iron retention in macrophages leads to lower iron availability for neighbouring cells, thus compromising the trophic role of macrophages, in the proliferative phase. This reduced iron availability could negatively influence the growth rate of various cell types (fibroblasts, epithelial and endothelial cells) and consequently the new tissue formation. To this regard, it is

important to remember the fundamental role of iron in collagen biosynthesis [52].

2.4 Macrophages in liver fibrosis

Liver fibrosis is an aberrant wound-healing process, characterized by the accumulation of ECM in the hepatic parenchyma, caused by increased production (fibrogenesis) or by inadequate degradation (fibrolysis) of ECM. Fibrosis represents the common end point of various hepatic insults, such as viral hepatitis, alcoholic and non-alcoholic fatty liver disease (NAFLD) [1]. In particular, NAFLD is the most prevalent liver disease in Western clinical practice and frequently evolves in non-alcoholic steatohepatitis (NASH), liver fibrosis, and hepatocellular carcinoma [53]. Physiologically, upon liver damage, inflammatory cells are activated: these include cells of the monocyte/macrophage lineage, both resident (Kupffer cells) and infiltrating [54-56]. The resulting inflammatory cascade leads to activation and proliferation of hepatic stellate cells (HSCs), a population of fibroblast-like cells resident in the space of Disse, which are primarily involved in extracellular matrix deposition (Figure 9): activated HSCs secrete collagen and express tissue inhibitors of metalloproteinases (TIMPs), thus resulting in matrix-degrading metalloproteinase activity inhibition. The consequent increased production of ECM, and its deposition in the space of Disse, cause alterations in liver architecture (such as the loss of endothelial fenestration and hepatocytes microvilli) and an impairment of normal metabolic exchange between portal venous flow and hepatocytes. These changes are normally transient and the regular structure is quickly restored, but, if the injury persists and becomes chronic, inflammation and accumulation of ECM continue and soon fibrogenesis exceed fibrolysis. This leads to the real process of fibrosis: a progressive substitution of liver parenchyma with scar tissue. The
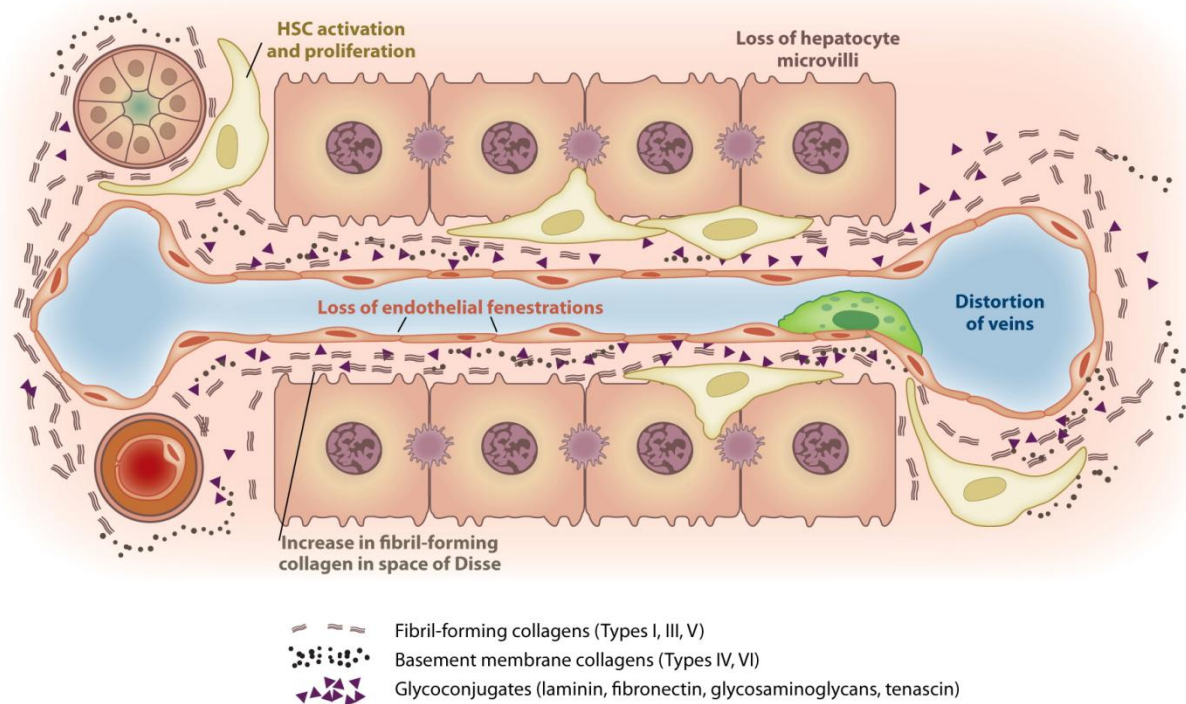
Figure 9. Matrix and cellular alteration in liver fibrosis.
Deposition of ECM in the space of Disse leads to the loss of endothelial fenestrations and hepatocyte microvilli, which results in the impairment of normal bidirectional metabolic exchange between portal venous flow and hepatocytes (Modified from [1]).

end consequence of continuous fibrosis is cirrhosis, the irreversible and complete loss of tissue architecture and function that represents a major cause of morbidity and mortality worldwide [1]. The main hypothesis of NAFLD progression to liver fibrosis is considered to be the augmented susceptibility to oxidative stress and inflammatory cytokines in fatty liver [57]. However, the molecular events and mechanisms responsible for this progression remain to be fully clarified. Experimental animal models can provide a great opportunity to bypass the environmental factors and genetic heterogeneity influencing NAFLD in humans. There are several diet-induced models of NAFLD in rodents; the methionine-choline deficient (MCD) diet is the most widely used in mice. It rapidly induces a pathological condition progressing from macrovesicular steatosis to hepatic fibrosis, depending on duration of the administration [58].

The role of both recruited monocytes and Kupffer cells in the process of liver fibrosis is crucial but controversial: they not only participate in the initial inflammatory response and induction of fibrogenesis, but seems also involved in fibrosis resolution [54-56].This ability of macrophages to act in both a pro- and anti-fibrotic manner has been partially explained by studies suggesting that these various functions may be performed by distinct macrophage populations (Figure 10). M1 macrophages appear to be pro-fibrotic [59],thanks to their production of oxygen radicals and pro-inflammatory cytokines. Conversely, M2 macrophages have a more controversial [54,60] role, depending on the specific subpopulation in which they differentiate. M2a-like macrophages, which produce cytokines that activate myofibroblasts (such as TGF-β), seem to support the progression

INFLAMMATION | RESOLUTION/FIBROSIS | FIBROLYSIS

M1 **M2**

a — c

Phagocytosis, pro-inflammatory factors, apoptosis

Anti-inflammatory factors, fibrotic and angiogenic factors

Anti-fibrotic and anti- angiogenic factors

IL-12 TNFα INFγ
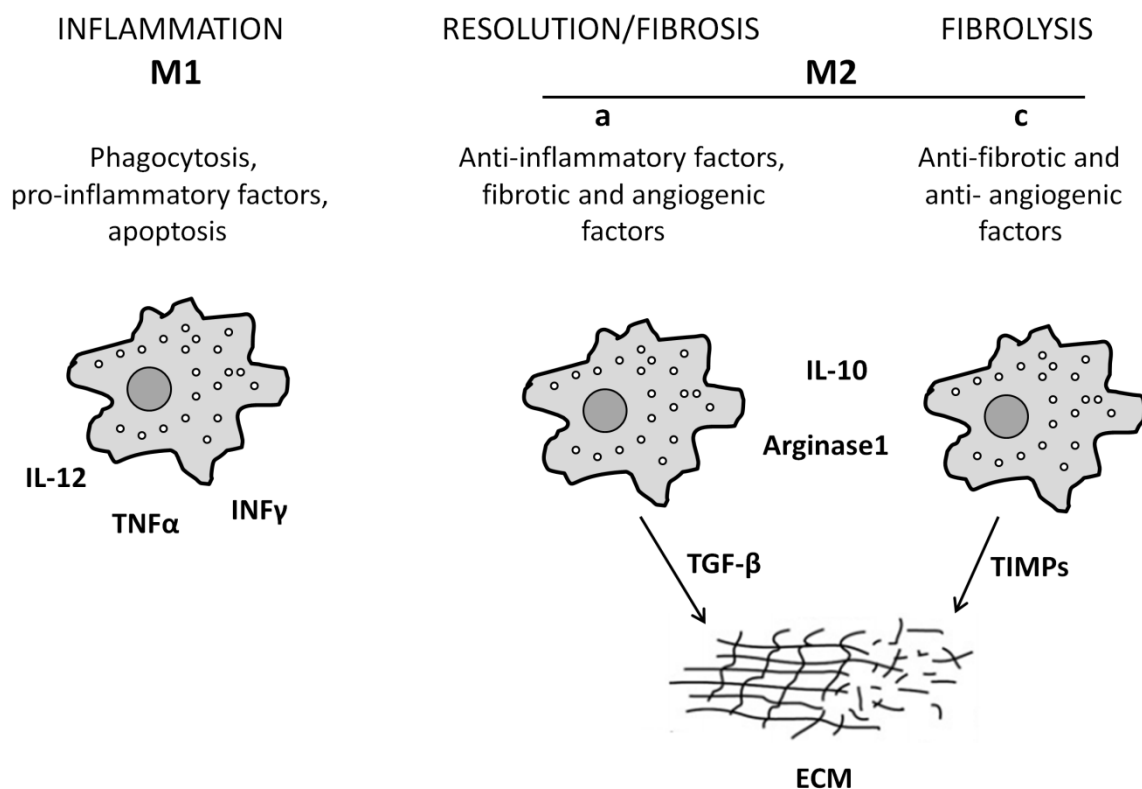
IL-10 Arginase1

TGF-β TIMPs

ECM

Figure 10. Different macrophage subpopulations have different roles in fibrosis.
M1 macrophages have a pro-fibrotic effect; M2a-like macrophages seem to support the progression of fibrotic disease, whereas differentiation into M2c-like macrophages, appears to promote fibrosis resolution.

of fibrotic disease; on the contrary, differentiation into M2c-like (or Mreg) macrophages promotes fibrosis resolution [56], by inhibiting M1, M2a-like and myofibroblasts activity through IL-10 and arginase1 production. The balance between different macrophage subsets, which depends on the microenvironment signals, seems to determine whether the outcome is resolution and healing or fibrosis.

2.4.1 Iron and fibrosis

Another possible explanation of the plasticity of macrophages in liver fibrosis could be the role of iron release or retention by macrophages. Numerous studies indicate that excessive iron stores worsen liver fibrosis [61]; Specifically, increased hepatic iron content is associated with the progression of liver disease in patients with hereditary hemochromatosis [62]. In this condition, the pathologic iron accumulation causes a process of lipid peroxidation in hepatocytes, leading to hepatocellular necrosis and aggravating the fibrotic state. In line with this concept, iron-removal therapies are effective lifesaving strategies. However, evidence that iron is a potent co-factor in the pathogenesis of fibrosis both in humans and animal models has been obtained mainly under conditions of increased total liver iron content and systemic iron overload [61]. Consequently, a harmful role of increased iron levels in selected cells has been proposed: redox active iron in hepatocytes, by catalyzing the formation of noxious ROS, may increase oxidative damage and affect signaling pathways involved in cell death and inflammation [63]. Moreover, it has been shown that iron overloaded Kupffer cells, in the presence of hepatocellular damage, are overactivated, greatly increase ROS production and may constitute a major drive to fibrosis [64]. In NAFLD, mild hepatic iron accumulation is seen in up to 30% of patients [65] and iron has been

implicated in cellular oxidative stress and insulin resistance, key features of NAFLD pathogenesis, and advanced fibrosis [66].

Still, it cannot be dismissed that liver fibrosis can be favoured also by an increased iron release by M2 macrophages. Indeed, the availability of iron in the extracellular environment is necessary for tissue growth and could influence the proliferation of adjacent fibroblasts and facilitate extracellular matrix deposition, in particular collagen synthesis [52]. Therefore, the role of macrophage-derived iron trafficking and compartmentalization in the process of liver fibrosis should be better clarified.

3. AIMS

Macrophages are essential in the inflammatory response. It is also known that iron metabolism is important in the context of inflammation and, in line with their different functions in homeostatic and inflammatory conditions, different macrophage populations differ in the expression of genes involved in iron homeostasis [29,30] as well as in the expression of immunoregulatory genes [31]. Understanding pathogenetic processes activated by altered macrophage iron trafficking could contribute to better understanding of how iron plays a major role in inflammation, and will hopefully help the development of novel therapeutic strategies.

Therefore, the aim of this project was to better understand the role of macrophage iron handling in inflammatory responses.

In particular, the study exploited a mouse model of impaired iron release from macrophages caused by cell-specific deletion of Fpn in order to try to:

1. Clarify the role of macrophage iron in cutaneous wound healing, a process characterized by a complex inflammatory response involving the presence, at different stages, of various macrophage polarized populations.

2. Investigate the role of macrophage iron in the context of liver fibrosis, a process with several analogies with cutaneous wound healing and in which iron seems to play an important role, using an experimental model recapitulating NAFLD, a diffuse pathology that may lead to fibrosis.

4. METHODS

4.1 Animals and dietary intervention

Mice carrying the floxed Fpn allele ($Fpn^{fl/fl}$) [12], kindly provided by Dr Nancy Andrews (Duke University), were bred to mice expressing Cre recombinase under the control of the macrophage-specific promoter Lysozyme M (LysM) in the C57BL/6J background (backcrossed for 10 generations) in order to generate mice with specific Fpn inactivation in monocyte–ma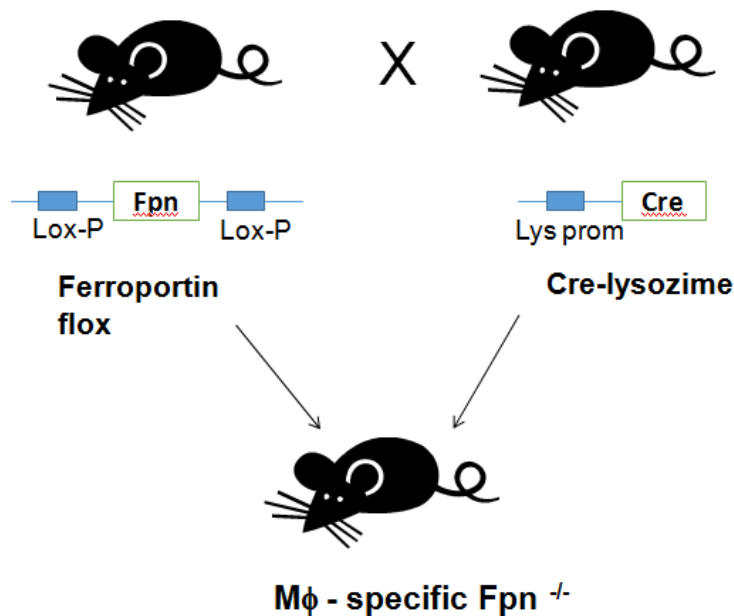crophage cell lineage ($Fpn^{fl/fl}Lys^{Cre/-}$)(Figure 11). $Fpn^{fl/fl}Lys^{Cre/-}$ mice were cohoused with littermates $Fpn^{fl/fl}Lys^{-/-}$ mice in individually ventilated cages in a specific pathogen–free animal facility at Humanitas Clinical and Research Center. Mice were typically maintained with normal diet (157 ppm iron content) and pups were weaned at 3 weeks of age. For the iron-deficiency, dams and pups were fed with an iron-deficient diet (9 ppm iron content; ssniff® EF R/M iron-deficient experimental diet, Charles River) from birth to 5 weeks after birth. Only some groups were given an iron-deficient diet for 11 weeks after birth, as indicated. Alopecia was quantified as follows: 100% = complete hair loss on the trunk; 50% = initial thin dorsal pelage; 0% = normal coat hair.

Figure 11. Genesis of a mouse model with a specific inactivation of Fpn in monocyte–macrophage cell lineage. Mice carrying a floxed Fpn allele were bred to mice expressing Cre under the control of the macrophage-specific promoter LysM in the C57BL/6 background.

Procedures involving animals handling and care were conformed to protocols approved by the Humanitas Clinical and Research Center in compliance with national (DL 116, GU suppl. 40, 18-2-1992; DL 26, GU 4-3-2014) and international law and policies (EEC Council Directive 2010/63/EU, OJ L 276/33, 22–09-2010; National Institutes of Health Guide for the Care and Use of Laboratory Animals, US National Research Council, 2011). The study was approved by the Italian Ministry of Health. All efforts were made to minimize the number of animals used and their suffering.

Genotyping was performed by PCR using the GoTaq Green Master Mix (Promega, Madison, WI) according to the manufacturer's protocol. Both the wild-type (350 bp) and the mutant alleles (700 bp) were identified by amplification with the same forward primer and a specific reverse primer (Table 1).

Table 1. Genotyping Primers

Primer Type	Sequence
Common forward primer	CTT GGG CTG CCA GAA TTT CTC
Wild-type reverse primer	TTA CAG TCG GCC AGG CTG AC
Mutant reverse primer	CCC AGA AAT GCC AGA TTA CG

4.2 Blood analyses

Blood was collected by cardiac puncture and Hb and Hct levels were immediately measured using a photometric analyser (HemoControl, EKF diagnostic, UK). Blood samples were centrifuged at 1500 g for 10 min at 4°C, and serum was stored at −20°C until analysis. Serum iron was measured using an UIBC/Iron kit (Thermo Scientific) and serum ALT and AST activity was determined using Reflotron® Plus system (Roche Diagnostics, Switzerland).

4.3 Skin wound healing model

To generate a punch wound, the back of anesthetized mice was shaved and exposed skin was cleaned with 70% ethanol. A full-thickness wound was created with a disposable 8-mm-diam biopsy punch by excising the skin and the underlying panniculus carnosus [67]. Gentamicin was immediately applied and upon histological analysis no gross infection was apparent through day 14. Wound sites of each mouse were digitally photographed and measured every day in the course of wound healing. The edges of the wounds were daily traced onto a transparency and the areas of open wounds were calculated using ImageJ software (v1.45q, NIH, USA). Changes of wound area over time were expressed as percentage of the initial wound areas. The animals were sacrificed at different times and skin biopsies were fixed with 4% paraformaldehyde, and embedded in paraffin or dehydrated with a sucrose gradient and embedded in OCT compound (Diapath, Bergamo, Italy) and stored at -80°C for histology or confocal microscopy analysis, respectively. Alternatively, skin biopsies were directly used for FACS and ELISA.

4.4 MCD diet model

Male 10-week-old C57BL/6 mice were randomly allocated into 2 groups. Mice in the MCD group (n=24) were fed on the MCD diet (Laboratori Dottori Piccioni) for 8 weeks. Control group (n=12) was fed on a methionine-choline-sufficient control diet, supplemented with choline chloride (2 g/kg diet) and D,Lmethionine (3 g/kg diet). Animals were sacrificed at 18 weeks. Livers were dissected out, examined for macroscopic lesions, frozen and kept at − 80 ∘C for RNA and protein extraction. A portion of the liver was immediately fixed with 4% paraformaldehyde and embedded in paraffin for histological analysis.

Blood was collected by cardiac puncture, centrifuged and serum stored for transaminases analysis.

4.5 Primary cell cultures

Bone marrow derived macrophages (BMDM) were generated as previously reported [68]. Briefly, bone marrow aspirates from femur of 8 to 12 week old mice were harvested and flushed out with Iscove modified Dulbecco medium (IMDM), 10% fetal calf serum (FCS) (Euroclone, Pero, Italy). After addition of ACK lysis buffer (Thermo Scientific, Milano, Italy) for red cells lysis, bone marrow cells where left to adhere overnight. Non-adherent cells were centrifuged and suspended at 0.5×10^6 cells/mL in complete bone marrow macrophage medium (IMDM, 10% FCS, 150 µM MTG, 10 ng/mL M-CSF) and cultured for 7 days. BMDM were stimulated by changing the medium to IMDM, 10% FCS, 150 µM MTG, 1% P/S, 1% L-glutamine, and 100 ng/mL LPS plus 20 ng/mL IFNγ or 20 ng/mL IL-4 for 24 h. Peritoneal exudate cells (PEC) were recovered from the peritoneal cavity of mice injected with 1 ml of 3% (wt/vol) dithioglycolate (Difco, BD Biosciences, Milano, Italy) as previously reported [69]. Briefly, 4-5 days after treatment, peritoneal cells were recovered in 5 ml of saline, centrifuged at 400 x g for 8 minutes, and cultured for 1 h in RPMI medium. After washing with phosphate buffered saline (PBS), adherent macrophages were cultured in RPMI containing 10% FCS.

4.6 Histopathological analysis

Organs and tissues were examined for gross lesions, trimmed after complete fixation and processed for paraffin blocks embedding. For histopathological analysis, 4 µm thick tissue sections obtained from the paraffin blocks were stained with hematoxylin and eosin. For necroinflammation and steatosis grading, hematoxylin and eosin stained

liver section were ranked as follow: 0 = absent; 1 = sparse or mild; 2 = noticeable; 3 = severe. For iron detection, 4 μm sections from each sample were stained with Perls' Prussian blue stain and semi-quantitatively evaluated under a light microscope as follows: 0 = absence of iron laden cells; 1 = rare iron laden cells; 2 = small number of iron laden cells; 3 = moderate numbers of iron laden cells; 4 = large numbers of iron laden cells. For fibrosis evaluation, 4 μm liver sections were stained with Sirius Red stain and evaluated as follows: 0 = absence of fibrosis; 1 = mild perisinusoidal fibrosis; 2 = moderate perisinusoidal fibrosis.

4.7 ELISA assay

Whole wounds were collected at 2, 7, and 12 days after wounding and homogenized in 50 mM Tris-HCl, pH 7.5, containing 2 mM EGTA, 1 mM PMSF, 100 KU aprotinin, 1% Triton X-100 (all from Sigma-Aldrich, Milano, Italy), and complete protease inhibitor cocktail (Roche, Monza, Italy). Total proteins were measured by DC Protein Assay, according to manufacturer's instructions (Bio-Rad Laboratories, Segrate, Italy). Cytokine levels were measured in accordance with the manufacturer's instructions (R&D Systems, Space, Milano, Italy). A seven-point standard curve was used to calculate the concentration of the molecules and PBS plus 1% BSA was used as a negative control. Absorbance was measured using GloMax® Discover Microplate Reader (Promega, Madison, WI) and analyzed using Prism software (version 6.00 for Windows; GraphPad).

4.8 Flow cytometry and cell sorting

A single-cell suspension of wounded skin was generated by cutting samples into small pieces and digestion in PBS (pH 7.4) supplemented with collagenase type I (1 mg/ml; Sigma-Aldrich) and hyaluronidase (125

U/ml; Sigma-Aldrich) at 37°C for 1 h, twice. Finally, a single-cell suspension was obtained by mechanical separation followed by 100 μm filtration and erythrocyte lysis in 0.15 M NH4Cl, 10 nM KHCO3, 1 nM Na4EDTA, pH 7.2. The following fluorophore-conjugated antibodies were used for immunophenotyping and intracellular staining: anti–mouse CD45 BV605TM (#30-F11; BD Biosciences); anti–mouse Ly6G PE-CF594TM (#1A8; BD Biosciences); anti–mouse Ly6C BV421TM (#AL-21; BD Biosciences); anti-mouse CD11b PerCP-CyTM5.5 (#M1/70; BD Biosciences); anti-mouse F4/80 PE-Cy7TM (#BM8; BioLegend, Campoverde, Milano, Italy); anti-mouse CD3 APC (#145-2C11 eBioScience, Thermo Fisher); anti mouse MHCII BV711 (#M5/114 BD Biosciences); CD206 PE (#C068C2 BioLegend); CD195 FITC (CCR3) (#J073E5 BioLegend). Dead cells exclusion was performed using LIVE /DEAD fixable Aqua dead cell stain kit (Life Technologies, Thermo Fisher) at room temperature for 15 minutes following the manufacturer instructions. All gated regions were restrictively defined using Fluorescence Minus One as negative control. Stained cells were analysed and/or sorted using FACS LSR Fortessa flow cytometer (BD Biosciences) or BD FACSAria III cell sorter (BD Biosciences). Diva software 20 (Version 8.0.1) (BD Biosciences) was used for data acquisition and analysis. The purity of sorted cells was ≥ 98%.

4.9 Confocal microscopy

Cryostat sections were incubated in 5% of normal goat (Dako, Milano, Italy) or donkey (Sigma-Aldrich) serum, 2% BSA, 0.1% Triton X-100 (Sigma-Aldrich) in PBS with calcium and magnesium chloride (PBS2+) pH 7.4 for 1 h at room temperature. Specimens were incubated with the following primary antibodies for 2 h at room temperature: rat monoclonal anti-PDGFR (#4C54, 2 μg/ml; Cell Sciences); rabbit polyclonal anti-collagen I (4 μg/ml; AbCam, Euroclone); Cy3-conjugated mouse monoclonal anti-

α-SMA (#1A4, 2 μg/ml; Sigma-Aldrich); rabbit monoclonal anti-Ki67 (#D3B5, 1:400; Cell Signaling Technology, Euroclone); rat monoclonal anti-CD31 (#MEC 13.3, 1 μg/ml; BD Biosciences); rabbit polyclonal anti-Lyve-1 (2 μg/ml; AbCam, Euroclone). Sections were then incubated for 1 h with Alexa Fluor® (488, 594, 647)-conjugated species-specific cross-adsorbed detection antibodies (Thermo Fisher Molecular Probes). For DNA detection, DAPI (300 nM; Thermo Fisher-Molecular Probes) was used. After each step, sections were washed with PBS2+ pH 7.4 containing 0.01% (vol/vol) Tween 20. Sections were mounted with the antifade medium FluorPreserve Reagent (EMD Millipore, Vimodrone, Italy) and analyzed with an Olympus Fluoview FV1000 laser scanning confocal microscope (Olimpus, Segrate, Italy). Immunoreactive areas were measured using the computer-assisted digital image processing software Image-Pro Plus (version 7.0; Media Cybernetics). The total stained area was automatically selected on the basis of RGB color segmentation and results are expressed as mean percentage of the immunoreactive area ± SD.

4.10 Quantitative real-time polymerase chain reaction (qRT-PCR)

Total RNA from liver, spleen, PEC or BMDM was extracted with TRI reagent® (Sigma-Aldrich) according to the manufacturer's instructions. The RNA concentration and quality were measured using an optical Nanodrop ND2000 spectrophotometer (Thermo Scientific). Total RNA (1000 ng) was reverse transcribed into cDNA with Proto Script M-MuLV First Strand cDNA Synthesis Kit® (New 21 England Biolabs, Euroclone) and the obtained cDNA served as a template for Real-Time PCR, based on the TaqMan® methodology (Life Technologies, Thermo Fisher) using a Corbett Rotor-Gene 3000 (Quiagen). Thermal cycling parameters were 40 cycles at 95° C for 15s and 60° C for 1 min. Each sample was amplified

in triplicate using the primers reported in Table 2 (Applied Biosystems, Thermo Fisher) and the amount of RNA was calculated using the $2^{-\Delta Ct}$ method. Results were normalized to 18S RNA and the housekeeping gene ribosomal protein large P0 (RPLPO) with similar results (in the figures only 18S RNA is shown).

Table 2. List of Primers

Gene	TaqMan gene expression assay ID
TfR1	Mm00441941_m1
Fpn	Mm01254820_m1
Rn18s	Mm03928990_g1
FtH	Mm04336019_g1
Fam132b	Mm00557748_m1
Arg1	Mm00475988_m1
TNFα	Mm00443260_g1
iNOS	Mm00440502_m1
Hepcidin	Mm04231240_s1
CD163	Mm00474091_m1
YM1	Mm00657889_mH
Alpha SMA	Mm00725412_s1
CCL2	Mm00441242_m1
CD11b	Mm00434455_m1
COL1-a1	Mm00801666_g1
COL1-a2	Mm00483888_m1
HO1	Mm00516005_m1
IL1a	Mm00439620_m1
IL1b	Mm00434228_m1
IL6	Mm00446190_m1
TGF-β	Mm01178820_m1
TIMP1	Mm01341361_m1

4.11 Western blot and amido black staining

BMDM and PEC samples were homogenized in 10 mM Tris-HCl, pH 7.0, 1 mM $MgCl_2$ and the postnuclear supernatant fraction obtained by centrifugation at 2000g for 10 minutes was ultracentrifuged at 150000g for 20 minutes to pellet crude membrane fractions [70]. Equal amounts of proteins were separated by SDS-polyacrylamide gels and transferred onto Hybond membranes (Amersham Biosciences, Euroclone). Blots were incubated with antibodies against FPN (1:250; Alpha Diagnostic, DBA, Segrate, Italy) and HRP-conjugated secondary antibodies. The proteins were detected using an immunodetection kit (ECL Plus; Amersham Biosciences, Euroclone). The results were quantified using Image J (v1.45q, NIH, USA). Data were normalized to proteins stained with 0.1% w/v amido black solution (Sigma-Aldrich).

4.12 Statistical analysis

Results are expressed as mean ± SEM, as specified. Statistical significance between groups was assessed by unpaired two-tailed Mann-Whitney test or Student's t test with Prism software (version 6.00 for Windows; GraphPad). When more than two groups were present Kruskal-Wallis one-factor analysis of variance (ANOVA) test was performed.

5. RESULTS

5.1 Lack of Fpn leads to iron accumulation in macrophages

Mice carrying the floxed Fpn allele (Fpn^{fl/fl}) [12], were bred to mice expressing Cre recombinase under the control of the macrophage-specific promoter Lysozyme M (LysM) in the C57BL/6J background in order to generate mice with specific Fpn inactivation in monocyte–macrophage cell lineage (Fpn^{fl/fl}Lys[Cre/-]). A mouse line with Fpn inactivation in macrophages driven by the LysM Cre has been previously described [71]. These mice were maintained on the 129/SvEvTac background, whereas we maintained our animals in the C57BL/6 background by backcrossing for over 10 generations. Since iron metabolism can be quite different among various mouse strains [72-74], we characterized our mice and compared the phenotype with previously published results. Fpn^{fl/fl}Lys[Cre/-] mice were viable, were born in Mendelian ratios, reproduced normally and did not show significant differences in body weight compared to Fpn^{fl/fl}Lys^{-/-}. No evident differences between males and females were observed. Histological analysis of the major organs showed no differences between the two genotypes.

Fpn expression in bone marrow derived macrophages (BMDM) and peritoneal exudate cells (PEC) was assessed at the mRNA level by qRT-PCR and at the protein level by western blot: a >90% reduction of Fpn expression confirmed the correct gene inactivation (Figure 12A and 12B).
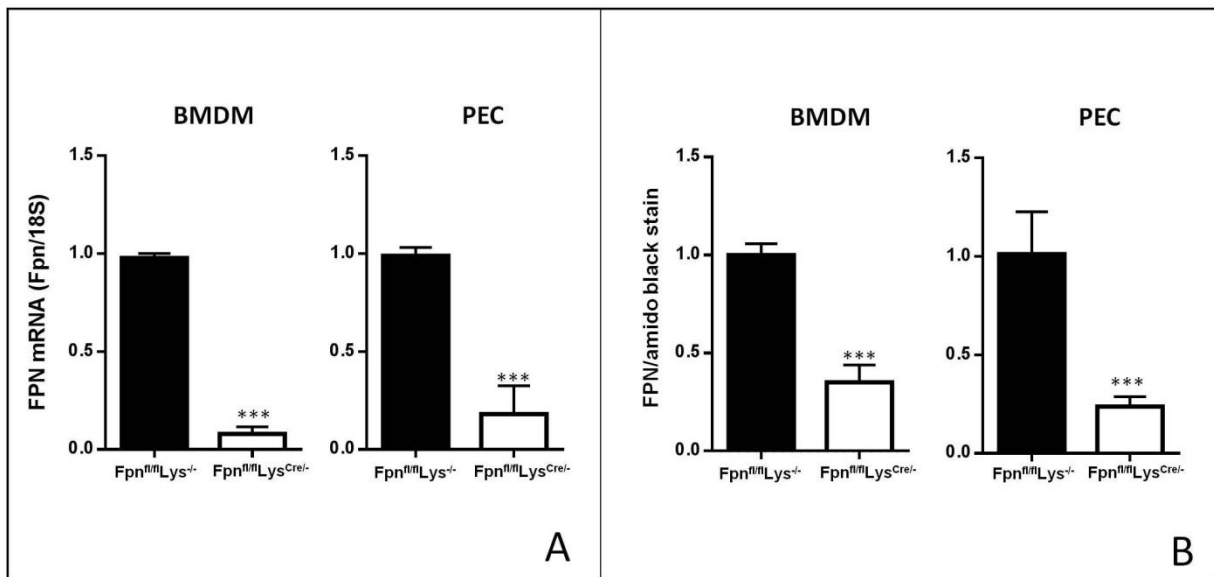
Figure 12. FPN deletion in BMDM and PEC of Fpn$^{fl/fl}$Lys$^{Cre/-}$ mice.

A) The inactivation of Fpn in macrophages was confirmed by qRT-PCRin BMDM and PEC of Fpn$^{fl/fl}$Lys$^{Cre/-}$ micevs littermates Fpn$^{fl/fl}$Lys$^{-/-}$. Results were normalized to the housekeeping gene 18S RNA(mean ± SEM of n=50 mice for each group; *** p< 0.0001).

B) Densitometric quantitation of immunoblot analysis of membrane Fpn in BMDM and PEC from Fpn$^{fl/fl}$Lys$^{-/-}$ and Fpn$^{fl/fl}$Lys$^{Cre/-}$mice. The blots were stained with amido black to assess equal protein loading (mean ± SEM of n=20 mice for each group; *** p< 0.0001).

Disruption of Fpn in macrophages led to iron accumulation, revealed by Perls' staining, in liver and spleen macrophages of Fpn$^{fl/fl}$Lys$^{Cre/-}$ mice compared to Fpn$^{fl/fl}$Lys$^{-/-}$ littermates (Figure 13).
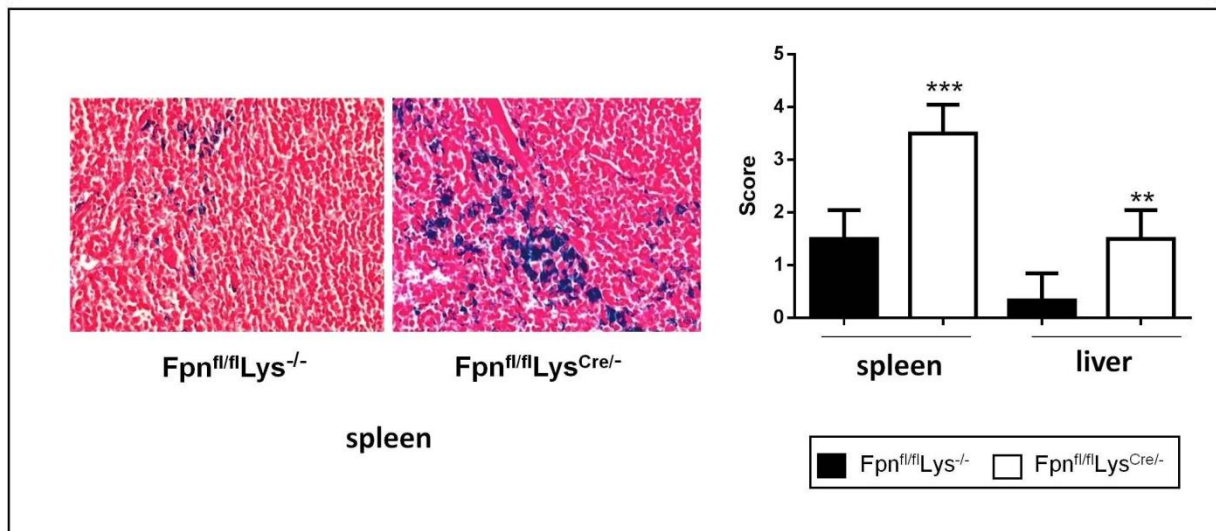
Figure 13. Fpn deletion causes iron accumulation in macrophages of Fpn^{fl/fl}Lys^{Cre/-} mice.

Histology of Perls' Prussian blue iron staining in paraffin sections of spleen from Fpn$^{fl/fl}$Lys$^{-/-}$ and Fpn$^{fl/fl}$Lys$^{Cre/-}$-mice. A semi-quantitative evaluation of Perls' iron staining in spleen and liver (performed as reported in Materials and Methods) is shown on the right. Data are presented as mean ± SEM of n= 6 for each group; *** $p< 0.0001$, ** $p< 0.001$. Magnification 40X

5.2 Lack of Fpn leads to transient anemia at 3 weeks after birth

As compared to control Fpn$^{fl/fl}$Lys$^{-/-}$ littermates, Fpn deletion in macrophages of Fpn$^{fl/fl}$Lys$^{Cre/-}$ mice resulted in a significant decrease in hemoglobin (Hb) levels and hematocrit (Hct) at 3 weeks after birth. Thereafter, both parameters rapidly returned to normal levels and remained almost unaltered until 18 weeks (Figure 14). On the contrary, serum iron levels do not show significant differences (Figure 14).
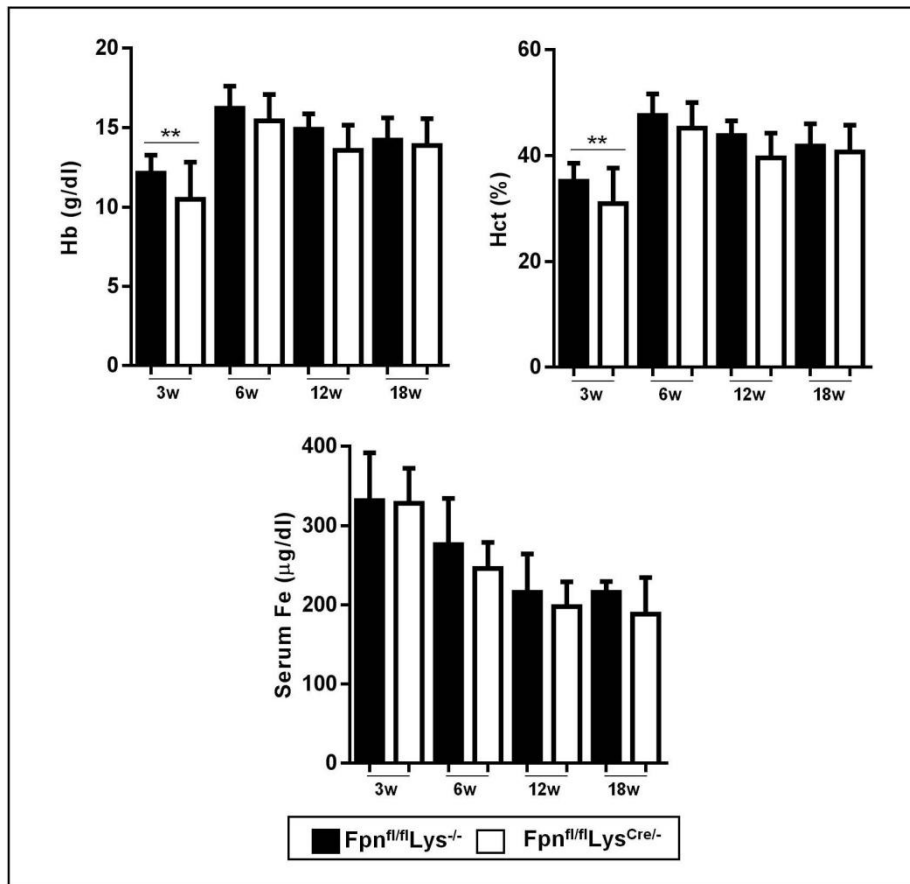
Figure 14. Fpn deletion in macrophages causes anemia in pups of Fpn^{fl/fl}Lys^{Cre/-} mice.

Hb levels, Hct and serum iron in 3, 6, 12, 18 week old mice. Hb and Hct showed a significant decrease at weaning, but returned to normal levels at 6 weeks and remained almost unaltered until 18 weeks (mean ± SEM of n=50 mice for each group; **p < 0.001).

The expression of HAMP, the main regulator of systemic iron metabolism, showed age-related variations but was not different in Fpn^{fl/fl}Lys^{Cre/-} mice compared to their control littermates (Figure 15). Accordingly, the expression of Fam132b mRNA encoding for erythroferrone, the erythroid regulator of HAMP [75], did not show significant differences (Figure 15).
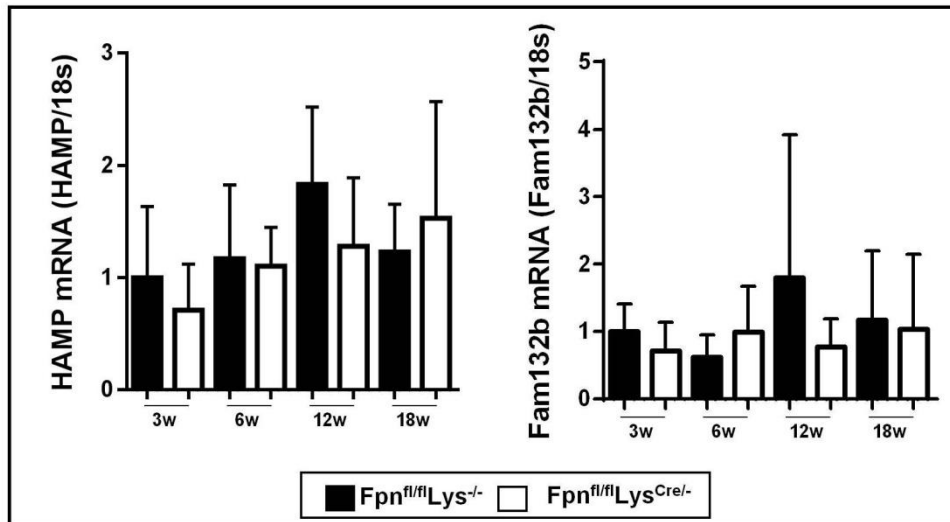
Figure 15. Expression of HAMP and Fam132b did not show significant differences between Fpn$^{fl/fl}$Lys$^{Cre/-}$ mice and controls.

HAMP and Fam132b expression of 3, 6, 12 and 18 week old mice. mRNA levels were measured by qRT-PCR and normalized to the housekeeping gene 18S RNA (mean ± SEM of n=10 mice for each group).

5.3 Fpn deletion in macrophages compromises hair follicle growth and causes alopecia

Fpn$^{fl/fl}$Lys$^{Cre/-}$ mice showed diffuse alopecia at birth without the involvement of the head; alopecia was present in both male and female mice and lasted until the fourth week of age (Figure 16A). Histological analysis in 3-week-old mice showed a moderate to severe coalescing dilatation of hair follicles, which contain remnants of hair shafts and keratin, and slight achantosis of the superficial epidermis (Figure 16A). Alopecia gradually disappeared and hair started to regrowth 2 weeks after weaning. Histological analysis showed that, despite hair regrowth, minor skin alterations were still detectable in adult (12 weeks) Fpn$^{fl/fl}$Lys$^{Cre/-}$ mice, with reduced number of hair follicles, multifocal areas of hair shafts rarefaction, and thin hypodermis with an apparent increase of adipose tissue (Figure 16B). Taken together, these results suggest that

Fpn deletion in macrophages causes severe alterations of the hair follicle and of the epidermis.
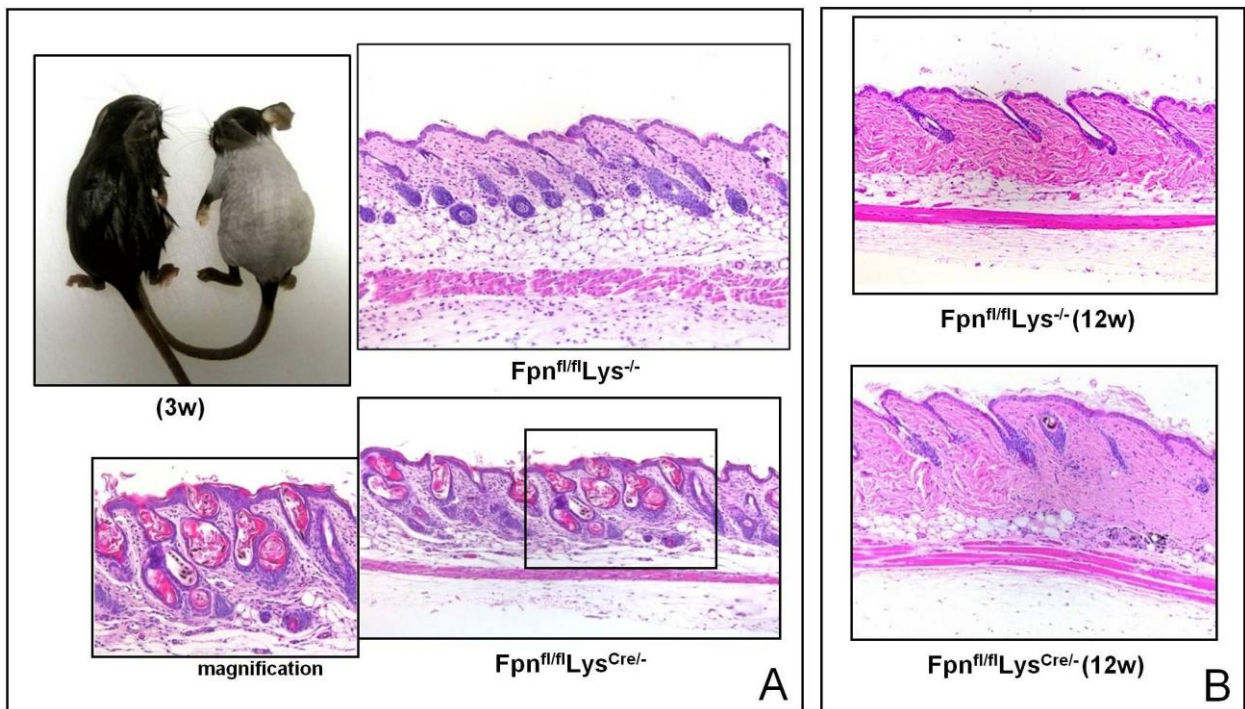

Figure 16. Transient alopecia is present in Fpn$^{fl/fl}$Lys$^{Cre/-}$ mice.

A) Appearance of 3-week-old Fpn$^{fl/fl}$Lys$^{-/-}$ (left) and Fpn$^{fl/fl}$Lys$^{Cre/-}$ (right) mice and histology (dorsal area) of the same mice. Tissue sections were stained with hematoxylin and eosin. Magnification 10X, in the inset 20X.

B) Histology of the skin (dorsal area) of adult (12-week-old) mice. Tissue sections were stained with hematoxylin and eosin. Magnification (10X).

5.4 Alopecia is not a direct consequence of anemia

The gradual disappearance of alopecia after weaning raised the possibility of a compensatory role provided by the switch in the diet, thanks to the higher iron availability. To better understand if alopecia in Fpn$^{fl/fl}$Lys$^{Cre/-}$ mice was a local reflection of systemic iron deficiency or a local effect of iron sequestration in macrophages, we determined the effect of an iron-restricted diet on the hair growth of both mice populations. We monitored hematologic parameters and alopecia in

pups fed for their first 3 weeks of life by dams kept on iron-deficient diet and then exposed to low iron diet for 2 additional weeks after weaning (Figure 17A). Until week 5, both Fpn$^{fl/fl}$Lys$^{Cre/-}$ and control littermates were anemic but Hb, Hct and serum iron levels were always significantly lower in animals lacking macrophage Fpn (Figure 17B and 17C).
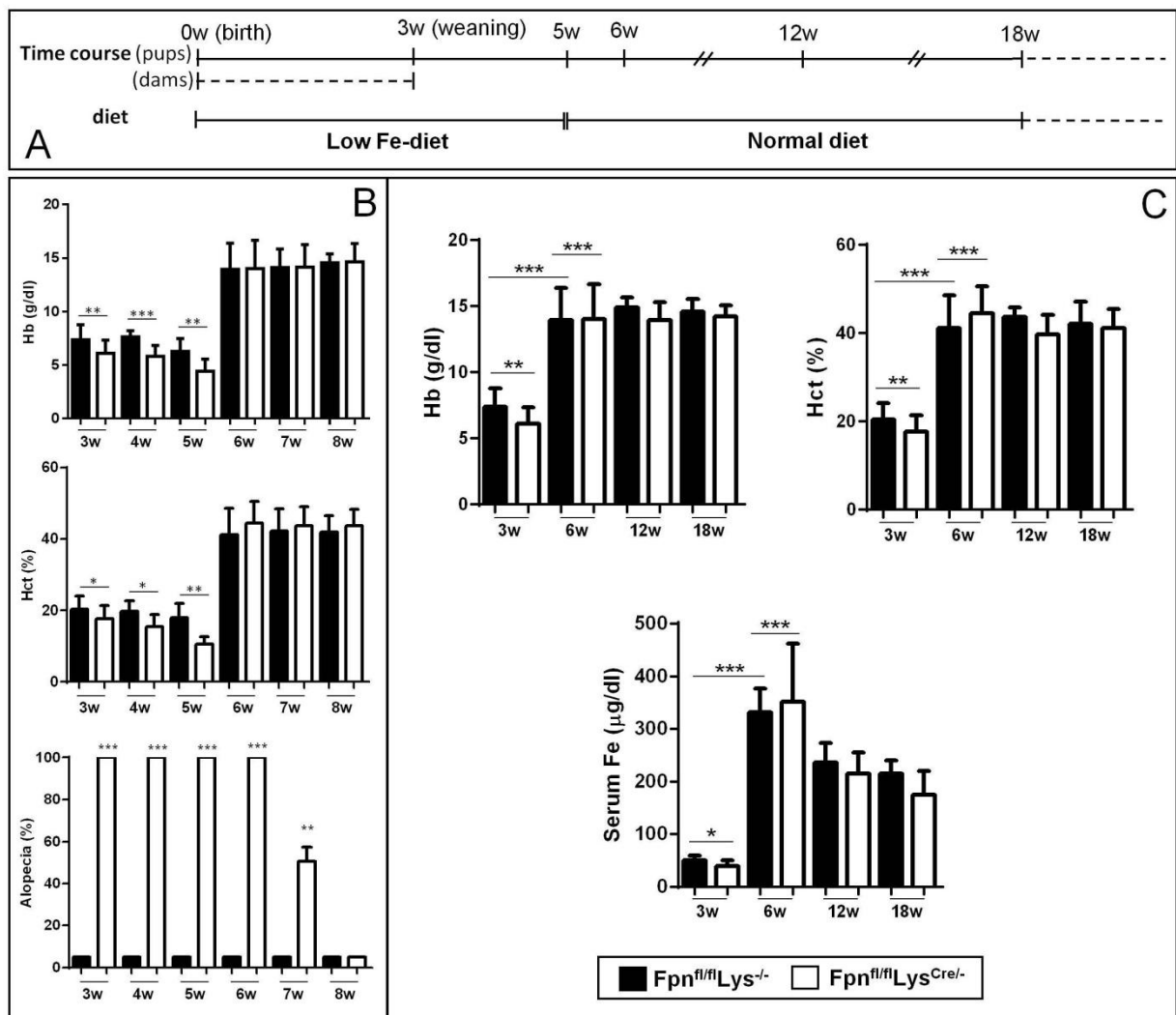

Figure 17. Alopecia in Fpn$^{fl/fl}$Lys$^{Cre/-}$ mice is not related to anemia.

A) Schematic overview of the feeding protocol: pups were fed by dams kept on iron-deficient diet for 3 weeks until weaning and then maintained on low iron diet for 2 additional weeks followed by normal diet.

B) Hb and Hct levels in 3-8-week-old mice (mean ± SEM of n=10 mice for each group; *** p < 0.0001, ** p < 0.001). The histogram at the bottom shows the degree of alopecia at different time points. *** p < 0.0001, **p < 0.001.

C) Hb, Hct and serum iron levels in 3-18-week-old mice (mean ± SEM of n=10 mice for each group; ** p < 0.001).

Mice with loss of macrophage Fpn were grossly affected by diffuse alopecia of the trunk, whereas Fpn$^{fl/fl}$Lys$^{-/-}$ mice did not develop alopecia during the period of exposure to the low iron diet (Figure 17B). Moreover, even exposing control mice to the iron deficient diet for 11 weeks did not trigger the appearance of alopecia. In Fpn$^{fl/fl}$Lys$^{Cre/-}$ mice, after the reintroduction of a normal diet, serum iron levels, Hb and Hct returned to normal levels 2 weeks before the restoration of normally haired skin (Figure 17B), thus indicating that alopecia and hypoferremia/anemia are not directly associated.

As expected, liver HAMP expression was repressed by the iron-deficient diet, but with no differences between Fpn$^{fl/fl}$Lys$^{Cre/-}$ mice and their control littermates (Figure 18). A significant increase in Fam132b expression was
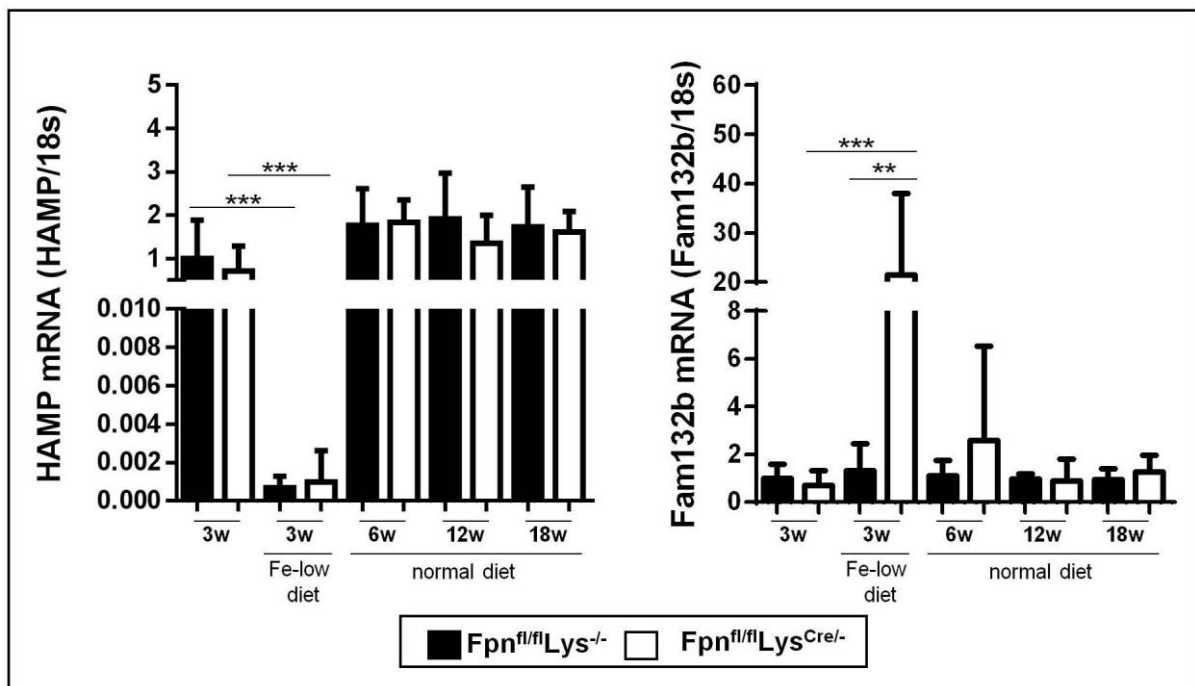

Figure 18. Expression of HAMP and Fam132b did not show significant differences between Fpn$^{fl/fl}$Lys$^{Cre/-}$ mice and controls.

HAMP and Fam132b mRNA levels in liver and spleen, respectively, of 3-18 weeks old mice. Expression in 3-week-old mice fed the normal diet is shown in comparison. mRNA levels were measured by quantitative RT-PCR and normalized to the housekeeping gene 18S RNA (mean ± SEM of n = 10 mice for each group; ** $p < 0.001$, *** $p < 0.0001$).

found in Fpn$^{fl/fl}$Lys$^{Cre/-}$ pups at 3 weeks (Figure 18), indicative of higher erythropoietic activity. After week 5, with the introduction of the normal diet, both HAMP and Fam132b expression returned to normal levels without differences between Fpn$^{fl/fl}$Lys$^{Cre/-}$ mice and controls (Figure 18).

Histological analysis confirmed that in Fpn$^{fl/fl}$Lys$^{Cre/-}$ mice alopecia was associated with severe follicular keratosis with intraluminal accumulation of keratin, distorted hair shafts and subsequent dilation of the hair follicles. Conversely, no relevant gross and histopathological changes were found in the dorsal haired skin of the Fpn$^{fl/fl}$Lys$^{-/-}$ mice maintained in the same dietary conditions (Figure 19A). In both mice populations, skin histology showed that hair follicles were in the anagen stage, but in Fpn$^{fl/fl}$Lys$^{Cre/-}$ mice hair shafts did not exit the follicular ostia and follicular
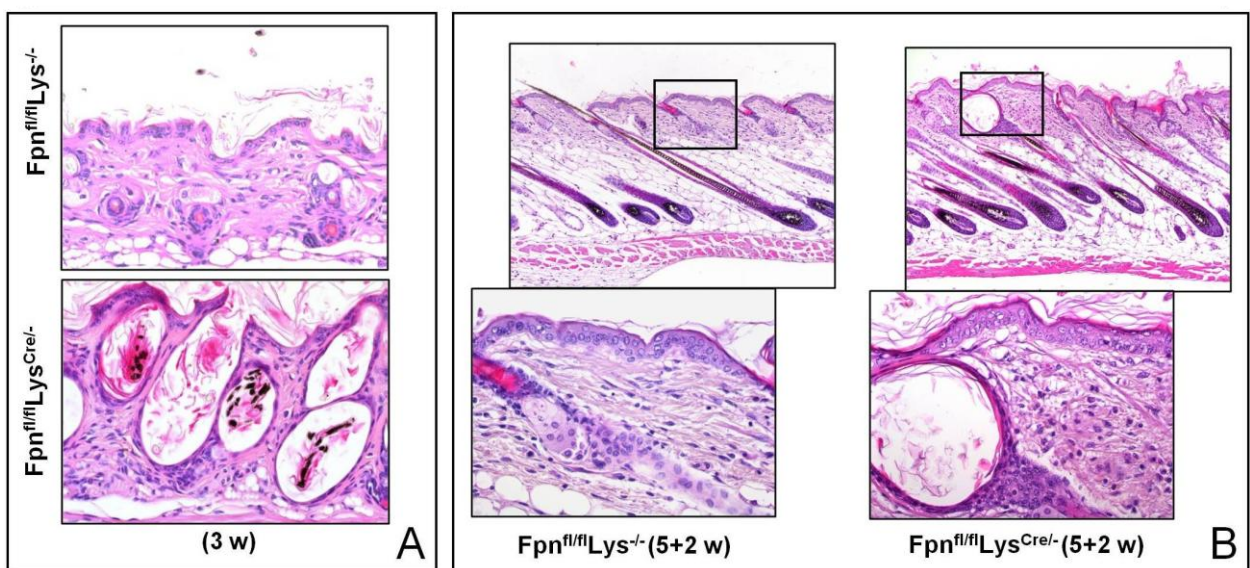

Figure 19. Fpn$^{fl/fl}$Lys$^{-/-}$ mice exposed to iron-deficient diet did not develop alopecia.

A) Representative histology of the skin (dorsal area) of 3-week-old Fpn$^{fl/fl}$Lys$^{-/-}$and Fpn$^{fl/fl}$Lys$^{Cre/-}$mice maintained with an iron deficient diet. Tissue sections were stained with hematoxylin and eosin. Magnification 20X.

B) Representative histology of the skin (dorsal region) after 5 weeks of iron deficient diet plus 2 weeks of normal diet. Tissue sections were stained with hematoxylin and eosin. Magnification 10X, in the insets 20X.

dilation, increased epidermal hyperplasia, and increased dermal inflammation were observed (Figure 19B).

We then investigated cell proliferation in hair bulb by analysing the expression of the cell proliferation marker Ki67 by confocal microscopy. Figure 20 shows a significant decrease of Ki67 expression in epithelial cells of the hair bulbs of 3-week-old Fpn$^{fl/fl}$Lys$^{Cre/-}$ mice compared to controls.
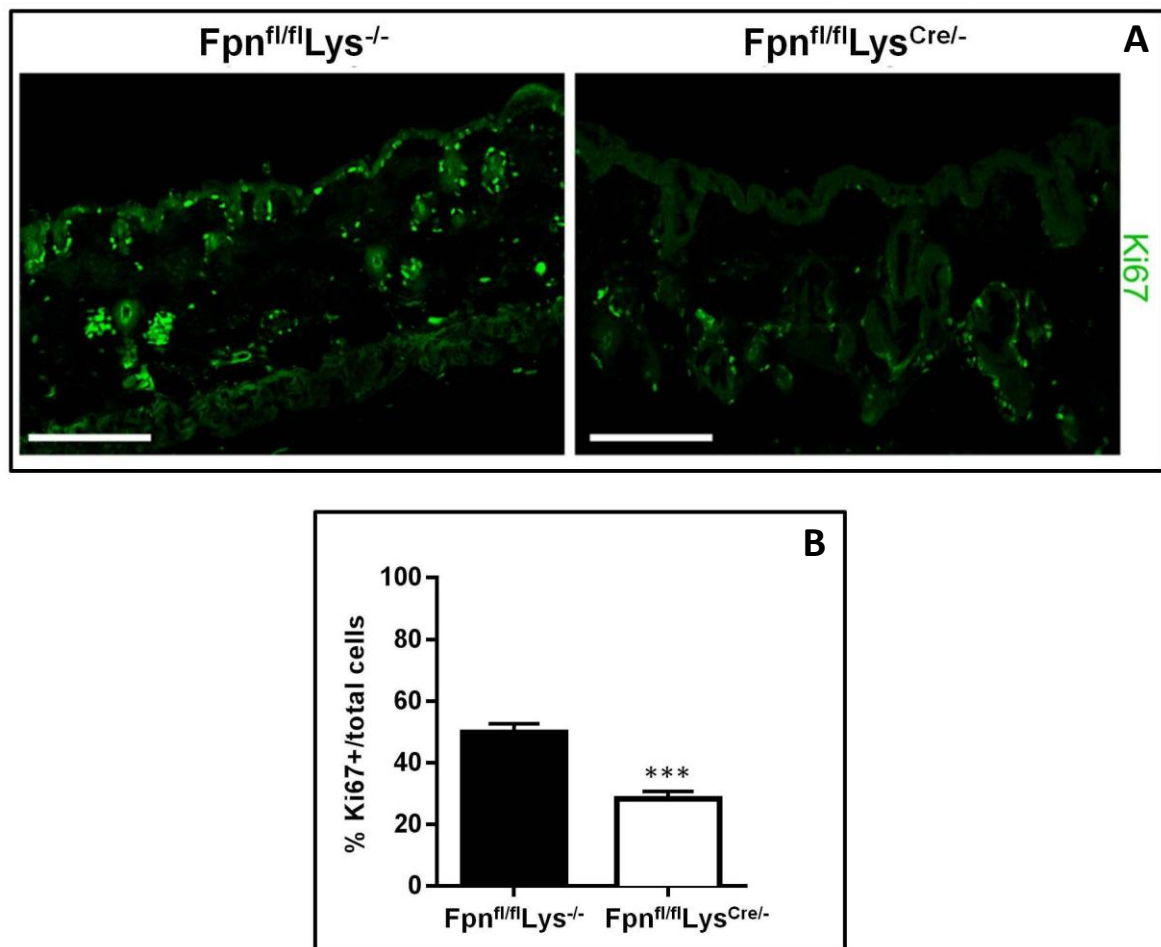

Figure 20. Decreased proliferation in cutaneous hair follicles of Fpn$^{fl/fl}$Lys$^{Cre/-}$ mice.

A) Expression and localization of Ki67 in cutaneous tissue of Fpn$^{fl/fl}$Lys$^{-/-}$ and Fpn$^{fl/fl}$Lys$^{Cre/-}$ mice was assessed by confocal microscopy. Bars, 100 µm. Magnification 40X.

B) Quantitation of confocal images, data are presented as mean ± SEM (5-9 field of vision/mouse, 3 mice/group); *** p< 0.0001

Interestingly, in the same cells we found a strong increase of TfR1 expression, indicative of cellular iron deprivation (Figure21). Conversely, macrophages (F4/80+ cells) did not expressed TfR1, confirming the iron-loaded status of these cells in $Fpn^{fl/fl}Lys^{Cre/-}$ mice. The great number of F4/80 positive cells in the skin (Figure 21) supports the critical role of macrophages in the homeostasis of this tissue.
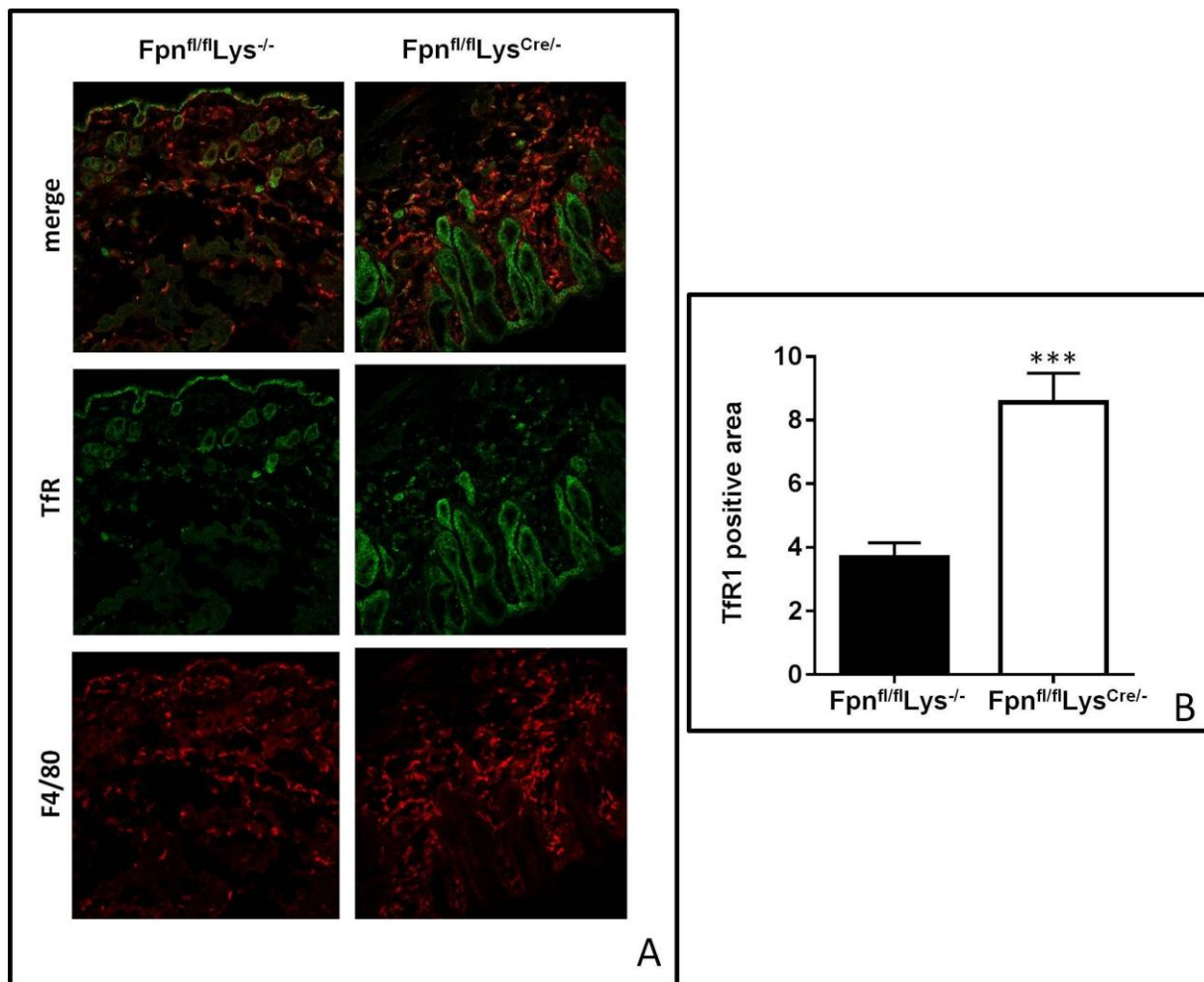

Figure 21. Increased iron demand in cutaneous hair follicles of $Fpn^{fl/fl}Lys^{Cre/-}$ mice.

A) Expression and localization of TfR1 and F4/80 in cutaneous tissue of $Fpn^{fl/fl}Lys^{-/-}$ and $Fpn^{fl/fl}Lys^{Cre/-}$ mice was assessed by confocal microscopy. Magnification 20X.

B) Quantitation of confocal images, data are presented as mean ± SEM (3 mice/group , 5-9 field of vision/mouse); *** p< 0.0001

Taken together, these results suggest that iron retention in resident macrophages has detrimental effects on tissue homeostasis by reducing iron availability for hair follicle cells and consequently inhibiting their proliferation.

5.5 Fpn deletion in macrophages affects cutaneous wound healing

To test the hypothesis that macrophage derived iron could be an important element in the context of tissue homeostasis, particularly under conditions of increased cell proliferation, we set-up a cutaneous wound healing model. After performing a full thickness incisional cutaneous wound, we monitored the entire time course of the repair process: the early-inflammatory (2 days post injury [dpi]), middle-proliferative (7 dpi), and late-remodeling phases (12 dpi). Macroscopical analysis showed that in Fpn$^{fl/fl}$Lys$^{Cre/-}$ mice the process of wound closure was considerably delayed as compared to wild-type littermates, with significantly wider lesions at all time points and a lag of 3-5 days in the wound closure (Figure22).
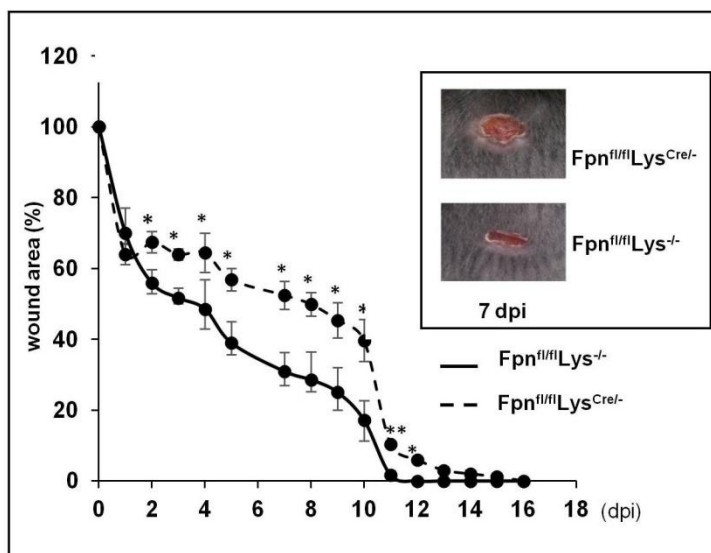

Figure 22. Skin repair is delayed in Fpn$^{fl/fl}$Lys$^{Cre/-}$mice.
Kinetic analysis of skin excisional wound areas. Values represent mean ± SEM of n= 24 for each group; * p< 0.01. One representative experiment (n= 6 mice/group) out of 4 is shown. The inset shows representative macroscopic images of Fpn$^{fl/fl}$Lys$^{-/-}$ and Fpn$^{fl/fl}$Lys$^{Cre/-}$ mice skin wounds at 7 dpi.

Histological analysis supported this observation, since Fpn$^{fl/fl}$Lys$^{Cre/-}$ mice displayed a more prolonged inflammatory response and delayed granulation tissue formation, whereas mononuclear cells and granulocytes were unchanged (Figure 23).
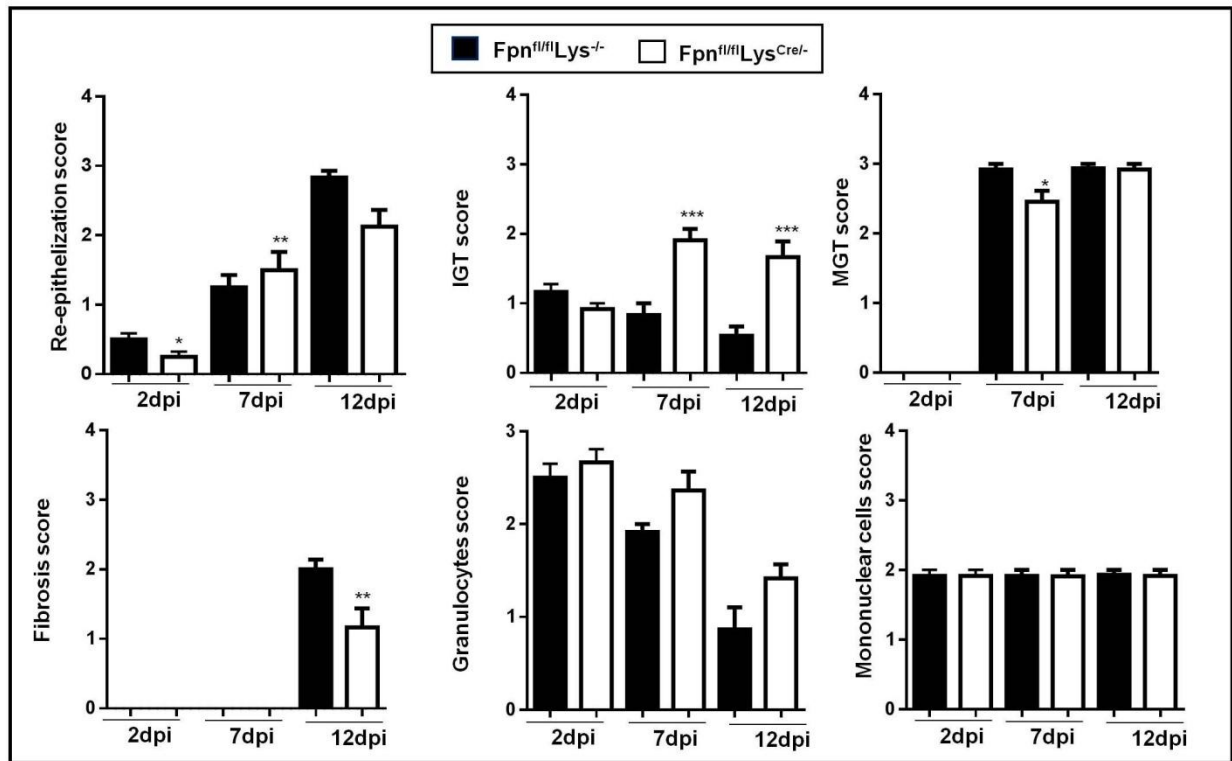
Figure 23. Fpn$^{fl/fl}$Lys$^{Cre/-}$mice displayed prolonged inflammatory response and delayed granulation tissue formation.

Histological grading of wound healing, based on separate evaluation of distinct features of wound healing process, at 2, 7, 12 dpi. IGT: Immature granulation tissue, MGT: mature granulation tissue. The semiquantitative score was defined as described in Supplemental Table 1; n= 12 for each group; *** $p < 0.0001$, ** $p < 0.001$, * $p < 0.01$.

5.6 Fpn deletion effectively causes iron accumulation in wound macrophages of Fpn$^{fl/fl}$Lys$^{Cre/-}$ mice

To characterize the functional impact of Fpn in the wound healing process, we first investigated its expression in FACS-sorted macrophages from wounds of control mice: Fpn mRNA levels were quite low in the inflammatory phase and progressively increased during the middle-late phases of repair (Figure 24), suggesting a predominant role of Fpn in the final phase of wound repair. The analysis of other iron related genes showed an increased expression of TfR1 and a decrease of Ft during the middle-late phases in macrophages obtained by wounded skin of control mice, but not from those obtained from Fpn$^{fl/fl}$Lys$^{Cre/-}$ mice, as a consequence of iron accumulation in these cells (Figure 24).
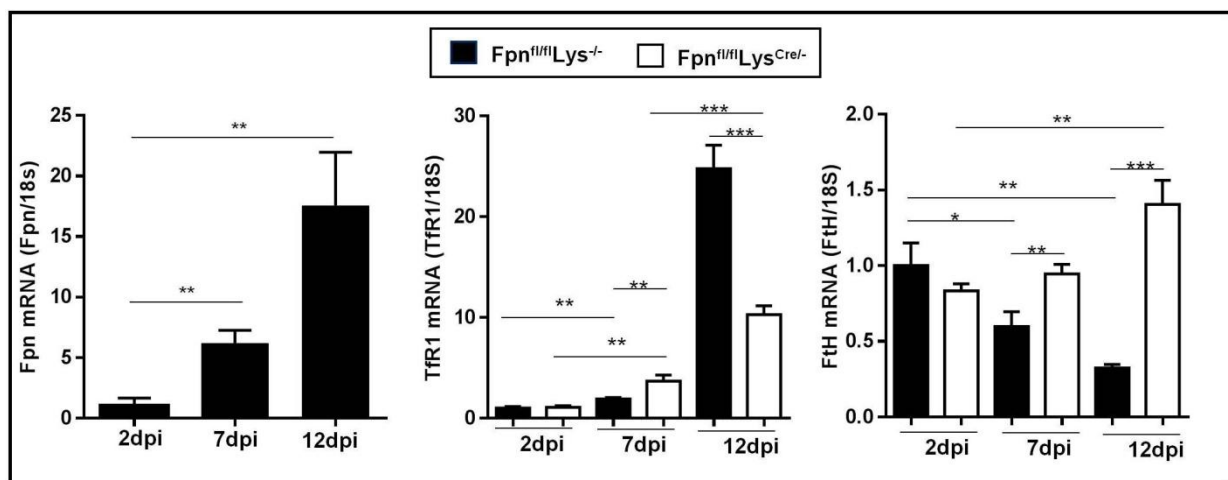

Figure 24. Iron release causes increased expression of TfR1 and a decrease of Ft in macrophages of control mice, but not of Fpn$^{fl/fl}$Lys$^{Cre/-}$mice.

Macrophages (CD45+/CD11b+/Ly6C+/F4/80+) were sorted by FACS from wounded skin tissue of 8 animals/group at 2, 7 and 12 dpi from Fpn$^{fl/fl}$Lys$^{-/-}$ and Fpn$^{fl/fl}$Lys$^{Cre/-}$ mice. Fpn, TfR1 and H-ferritin (FtH) mRNA expression was assessed by qRT-PCR and normalized to the housekeeping gene 18S RNA. Data are presented as mean ± SEM; * p< 0.01, **p<0.001, *** p < 0.0001

Accordingly, iron accumulation in macrophages localized in wounds of Fpn$^{fl/fl}$Lys$^{Cre/-}$ mice was confirmed by histological analysis (Figure 25).
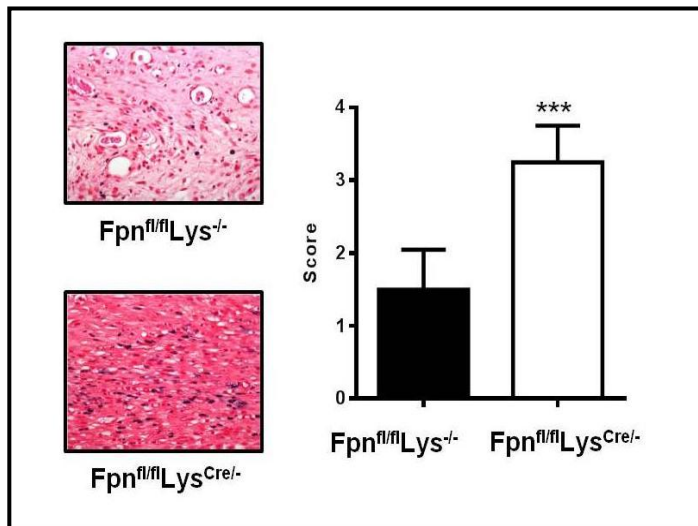
Figure 25. Fpn deletion causes iron accumulation in macrophages localized in wounds of Fpn$^{fl/fl}$Lys$^{Cre/-}$ mice.

Representative histology of Perls' Prussian blue iron staining of dorsal skin samples at 12 dpi in Fpn$^{fl/fl}$Lys$^{-/-}$ and Fpn$^{fl/fl}$Lys$^{Cre/-}$ mice. Magnification 40X. A semi-quantitative evaluation of Perls' iron staining is shown on the right. n= 6 for each group; *** p < 0.0001.

HAMP-dependent Fpn modulation does not seem to play a role in wound healing, as liver HAMP expression showed no differences between Fpn$^{fl/fl}$Lys$^{Cre/-}$ mice and controls during the entire time course of the wound repair process (Figure 26).
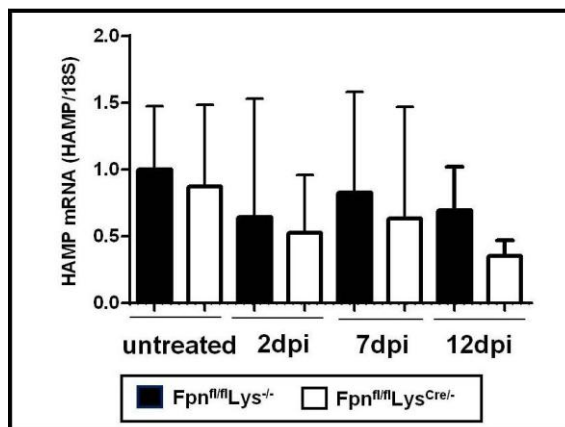

Figure 26. HAMP-dependent Fpn modulation is not involved in wound healing.

HAMP expression in liver of mice untreated and at 2, 7, 12 dpi. mRNA levels were measured by quantitative RT-PCR and normalized to the housekeeping gene 18S RNA. Data are presented as mean ± SEM of n=12 mice for each group.

5.7 Iron retention in macrophages has no impact on inflammatory response in cutaneous wound healing

As it has been reported that iron accumulation in macrophages might favour the expression of inflammatory mediators [51,71,76,77], we evaluated the levels of inflammatory cytokines in wound lysates, but we did not detect significant differences between the two mouse lines at any time point, with the only exception of increased levels of CXCL1 at 7 dpi in Fpn$^{fl/fl}$Lys$^{Cre/-}$ mice (Figure 27).
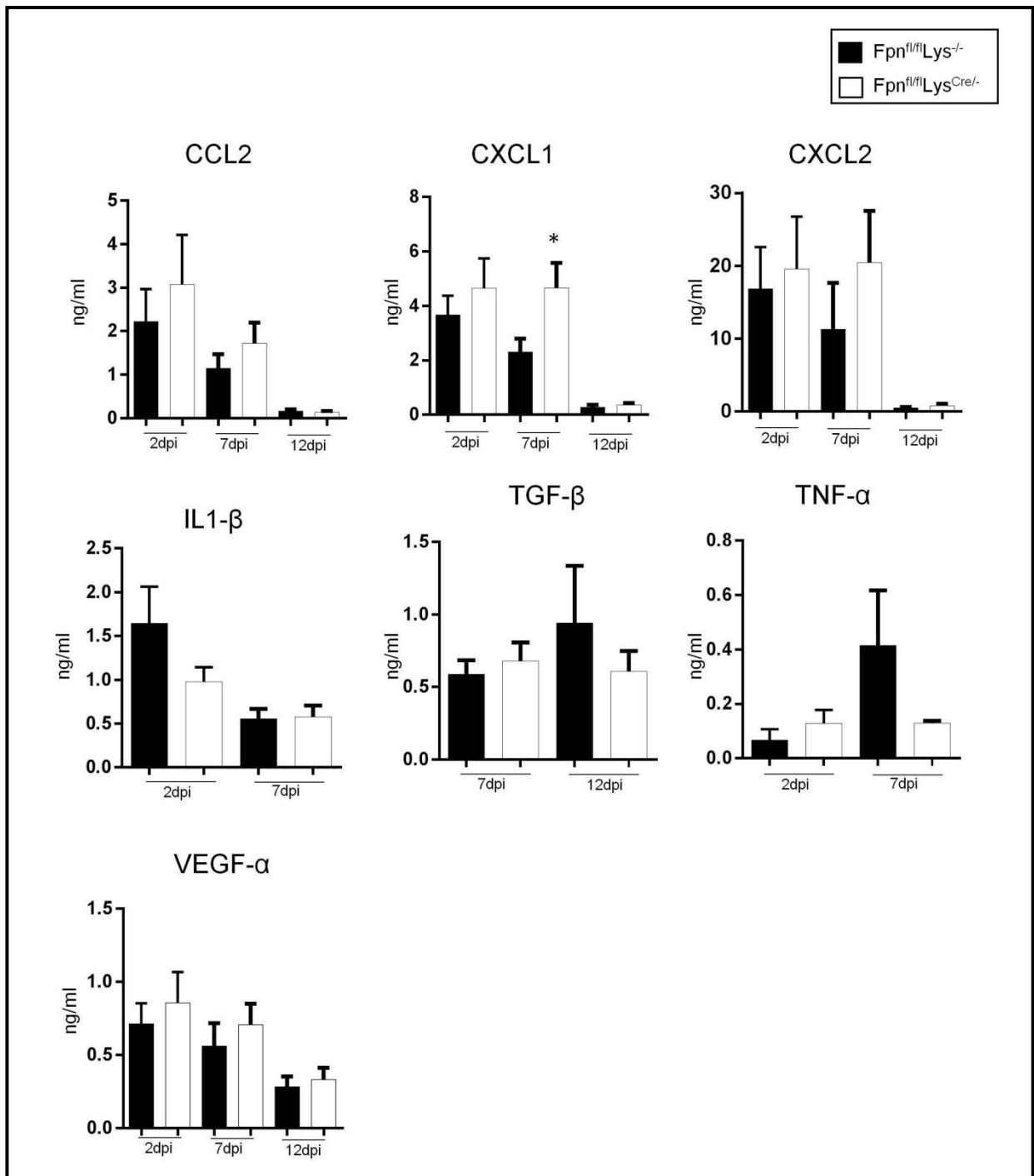
Figure 27. Cytokines levels in wound skin are not altered in Fpn^fl/flLys^Cre/- mice.

CCL2, CXCL1, CXCL2, IL-1β, TGF-β, TNFα and VEGFα protein levels in wound lysates from Fpn^fl/flLys^-/- and Fpn^fl/flLys^Cre/- mice were assessed by ELISA at different dpi after skin injury. At the time points not shown, the levels of the respective cytokine were below the detection limit of the assay. Data are presented as mean ± SEM; n=10 mice for each group; * p < 0.01.

Given the role of leukocytes in the orchestration of tissue repair [3], it was important to establish whether the defective wound healing observed in Fpn$^{fl/fl}$Lys$^{Cre/-}$ mice was the result of altered leukocyte recruitment. Analysis of leukocyte subsets showed that neutrophils (Ly6G+ cells) and eosinophils (CCR3+ cells) were abundant at 2 and 7 dpi and decreased thereafter (12 dpi), whereas an inverse trend was evident for T cells (CD3+ cells), which significantly increased at late time-points (12 dpi) (Figure 28). These cell accumulation kinetics, which are typical of skin wound healing [43], showed no differences in Fpn$^{fl/fl}$Lys$^{Cre/-}$ mice compared to controls, indicating that Fpn deletion in macrophages has no impact on leukocyte recruitment and activation in the wound.
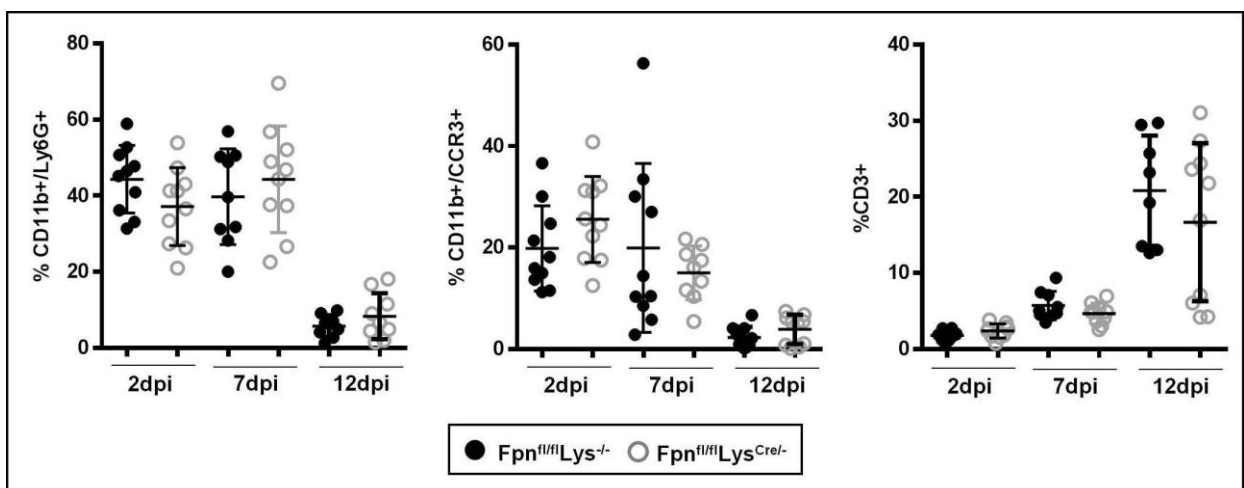
Figure 28. Wound infiltrating leukocytes are not altered in Fpn$^{fl/fl}$Lys$^{Cre/-}$ mice.

Frequencies of neutrophils (CD11b+/Ly6G+), eosinophils (CD11b+/CCR3+) and T lymphocytes (CD3+) on CD45+ cells. Dots and black lines represent single animals and the mean ± SEM, respectively; n=10 mice for each group; * p < 0.01.

Macrophages (F4/80+ cells) showed a trend similar to the one observed for T cells: a significant increase at 12 dpi (Figure 29). Since iron accumulation in macrophages could interfere with the polarization process during the healing process [29], we next investigated the

distribution of the different macrophage polarized populations during the time course of wound healing. As expected, FACS analysis showed an increase in macrophages expressing an M1 profile (MHCII+/CD206-) in the middle-proliferative phase, followed by a wave of macrophages expressing an M2 profile (MHCII-/CD206+) in the late-remodeling phase, but no difference was found between Fpn$^{fl/fl}$Lys$^{Cre/-}$ mice and their control littermates (Figure 29).
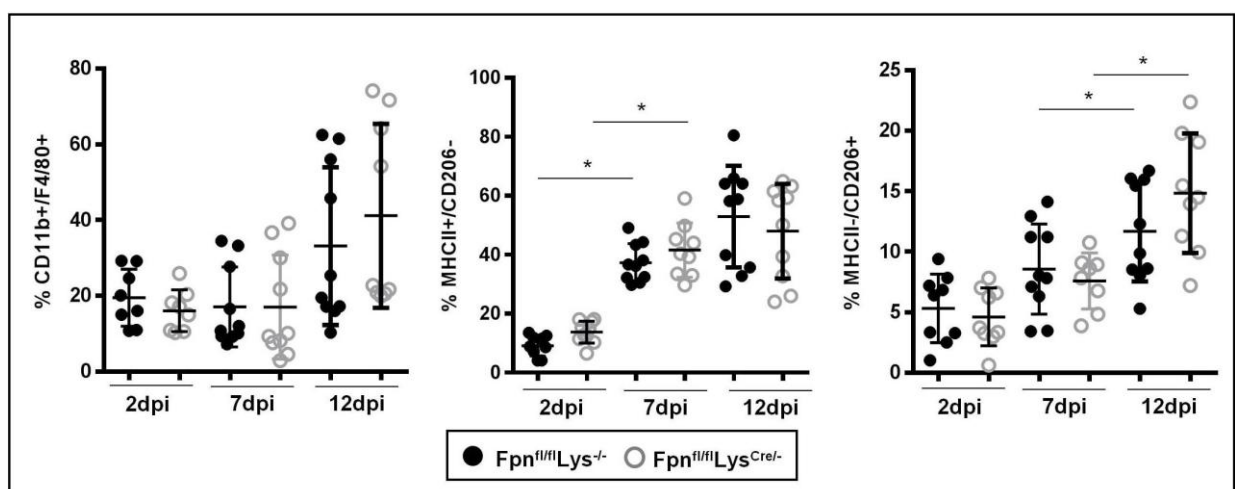
Figure 29. Fpn deletion does not modify macrophage polarization in Fpn$^{fl/fl}$Lys$^{Cre/-}$mice. Frequencies of macrophages (CD11b+/F4/80+) on CD45+ cells; frequencies of M1 (MHCII+/CD206-) and M2 (MHCII-/CD206+) polarized macrophages on total live macrophages. Dots and black lines represent single animals and the mean ± SEM, respectively; n=10 mice for each group; * p < 0.01.

To further investigate this aspect, we evaluated the effect of Fpn deletion on the expression of polarization markers in BMDM exposed to polarization stimuli in vitro, but again no difference was observed for neither M1 (iNOS and TNFα) or M2 (Arg1 and YM1) markers between Fpn$^{fl/fl}$Lys$^{Cre/-}$ and Fpn$^{fl/fl}$Lys$^{-/-}$ BMDM (Figure 30). These results indicated that, in this model, iron retention in macrophages has no impact on

leukocyte recruitment and activation as well as macrophage polarization, and the delay in wound closure is not a consequence of unaltered inflammatory component of the healing process.
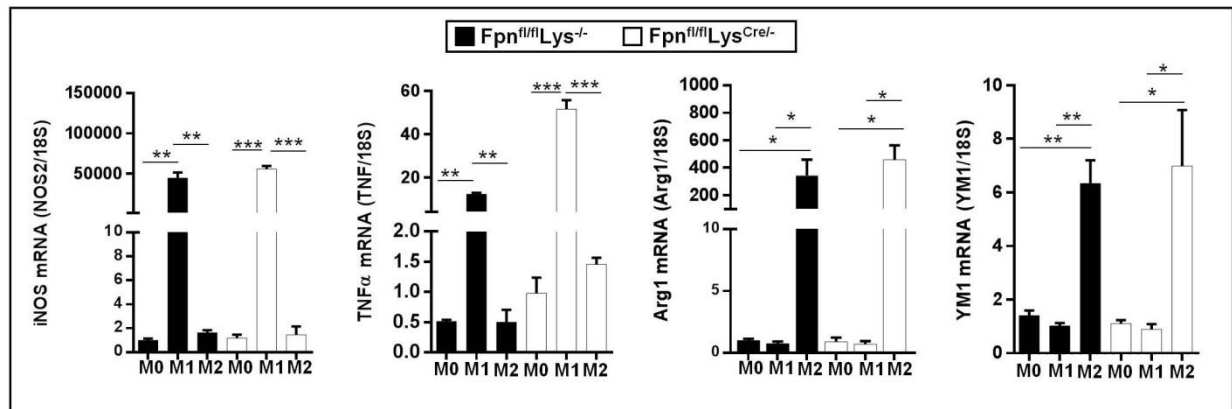
Figure 30. Fpn deletion does not modify macrophage polarization in BMDM derived from Fpn^{fl/fl}Lys^{Cre/-}mice and polarized in vitro.

BMDMs from Fpn$^{fl/fl}$Lys$^{-/-}$ and Fpn$^{fl/fl}$Lys$^{Cre/-}$ mice were polarized to M1 and M2 macrophages and relative iNOS, TNFa, Arg1 and YM1 mRNA levels were measured by qRT-PCR at 24 hours; results were normalized to the housekeeping gene 18S RNA (mean ± SEM of n=12 mice for each group; *** $p < 0.0001$, ** $p < 0.001$, * $p < 0.01$).

5.8 Fpn deletion in macrophages affects stromal cells during cutaneous wound healing

Since Fpn deletion in macrophages did not alter the inflammatory processes of wound healing, we then evaluated whether the defective iron release could affect stromal cells in the wound tissue. Confocal analysis at 7 dpi showed reduced expression in Fpn$^{fl/fl}$Lys$^{Cre/-}$ mice, as compared to control littermates, of blood (CD31) and lymph vessel (Lyve-1) endothelium markers (Figure 31).
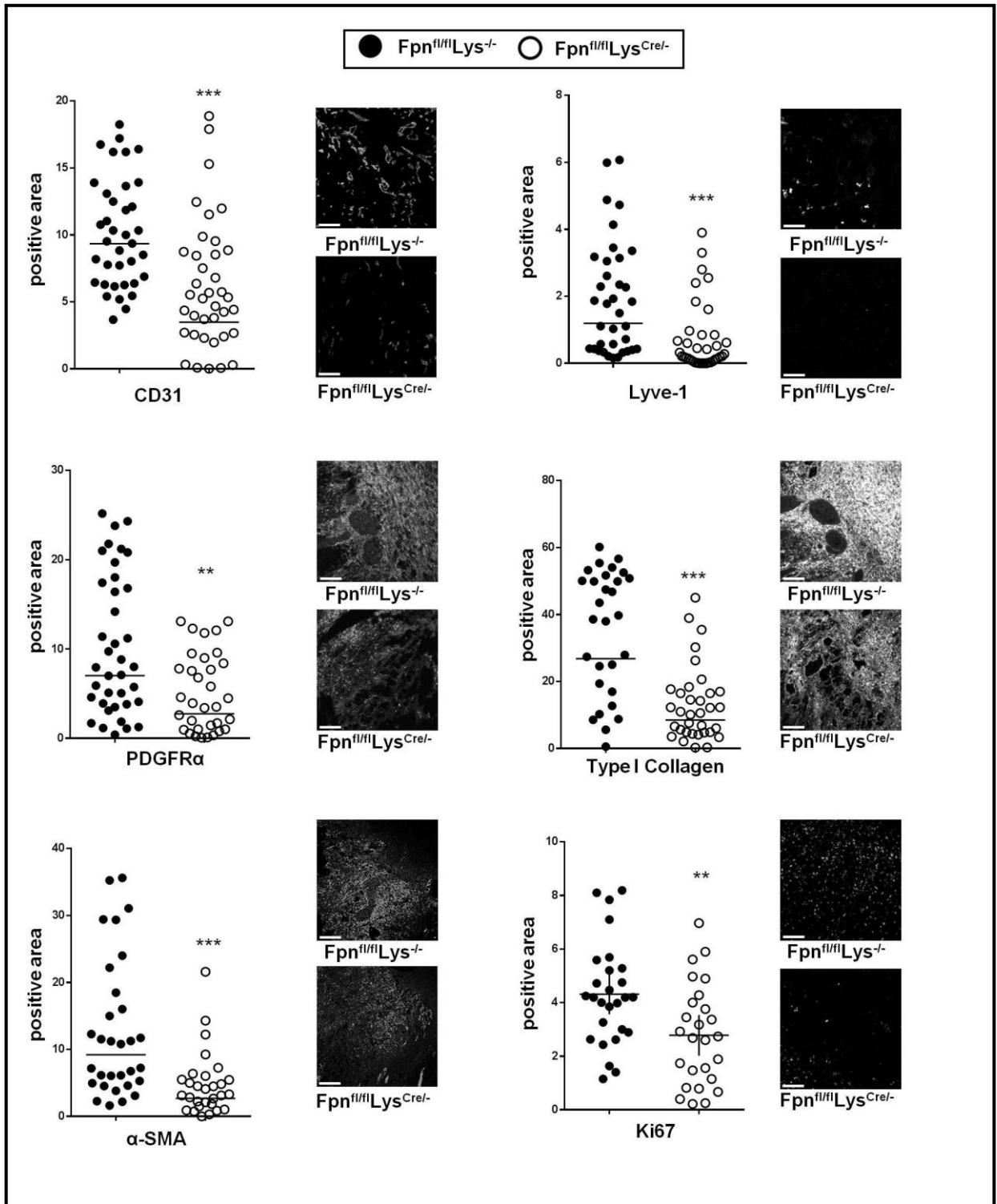
Figure 31. Vessel and stromal cells are reduced in Fpn^fl/fl^Lys^Cre/-^ mice.

Expression of CD31, Lyve-1, collagen-1, PDFGR, αSMA, Ki67 after skin wounding at 7 dpi was assessed by confocal microscopy and the positive area expressed as %. Each circle represents a single confocal image (5-9 field of vision/mouse, 6 mice/group; *** $p < 0.0001$, ** $p < 0.001$). Representative confocal microscopy images are shown. Bars, 100 µm. Magnification 40X.

This was accompanied by decreased expression of PDGFRα, a marker of mesenchymal cells, and lower levels of collagen I and αSMA, which are markers of activated fibroblasts and myofibroblasts, respectively (Figure 31). Moreover, loss of macrophage Fpn impaired cell proliferation, as shown by decreased Ki67 expression (Figure 31). Taken together, these results indicate that, though it does not interfere with immune cells recruitment and local activation, Fpn deletion in macrophages impairs blood vessels formation and stromal cells proliferation, leading to delayed skin repair.

5.9 Fpn deletion in macrophages does not affect steatohepatitis induced by MCD diet

After cutaneous wound healing, another useful model we decided to explore was liver fibrosis. To investigate how macrophage derived iron could influence this process, we set up a model of liver fibrosis via the widely used MCD diet model, which causes a liver injury similar to human NAFLD [78]. Choline deficiency induces lipid accumulation in the liver by impairing the synthesis of very low-density lipoprotein (VLDL) [79], an effect similar to methionine deficiency, which also causes oxidative stress and contributes to fibrosis progression [80].

In line with the results showed above (Figure 13), iron accumulation, revealed by Perls' staining, was evident in liver macrophages of Fpn$^{fl/fl}$Lys$^{Cre/-}$ mice compared to Fpn$^{fl/fl}$Lys$^{-/-}$ littermates, and the staining was not significantly affected by exposure to the control or MCD diet (Figure 32).
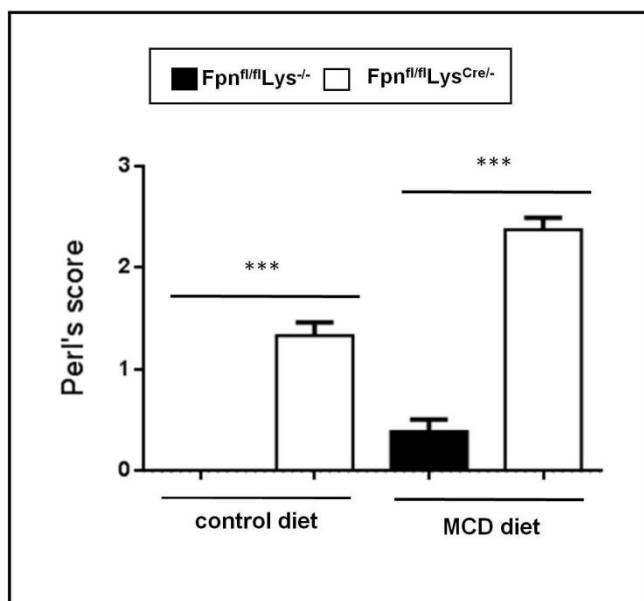
Figure 32. Fpn deletion causes iron accumulation in liver macrophages of Fpn$^{fl/fl}$Lys$^{Cre/-}$ mice.

Semi-quantitative evaluation of Perls' iron staining. n= 12 for each group; *** p < 0.0001.

As expected, animals exposed to the MCD diet presented a 3 to 5-fold increase in the levels of ALT and AST compared to animals fed the control diet (Figure 33). Interestingly, levels of both AST and ALT were significantly lower in Fpn$^{fl/fl}$Lys$^{Cre/-}$ mice fed the MCD diet compared to Fpn$^{fl/fl}$Lys$^{-/-}$ littermates exposed to the same diet, indicating a less severe cell damage(Figure 33).
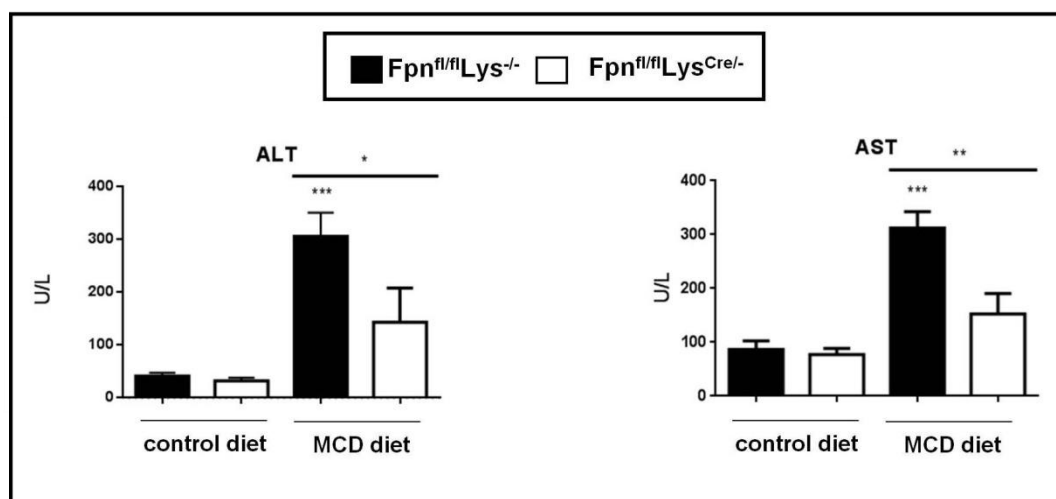
Figure 33. MCD diet in Fpn$^{fl/fl}$Lys$^{Cre/-}$mice causes less severe liver damage.

At the time of killing, blood was drawn and plasma levels of total protein ALT and AST were measured. Data are presented as mean ± SEM; * p< 0.01, **p<0.001, *** p < 0.0001.

We then tried to further investigate this aspect by performing histological analysis of liver sections from animals exposed to both control and MCD diets. As expected, when fed a control diet the livers of Fpn$^{fl/fl}$Lys$^{Cre/-}$ mice had a histological appearance indistinguishable from that of Fpn$^{fl/fl}$Lys$^{-/-}$ mice, and both showed no signs of steatohepatitis or fibrosis (Figure 34). On the contrary, the MCD diet produced severe steatosis and inflammation, but without significant differences between Fpn$^{fl/fl}$Lys$^{Cre/-}$ mice and control mice (Figure 34A). Blinded semi-quantitative evaluation of necro-inflammation and steatosis scores by an expert anatomopathologist confirmed this result (Figure 34B).
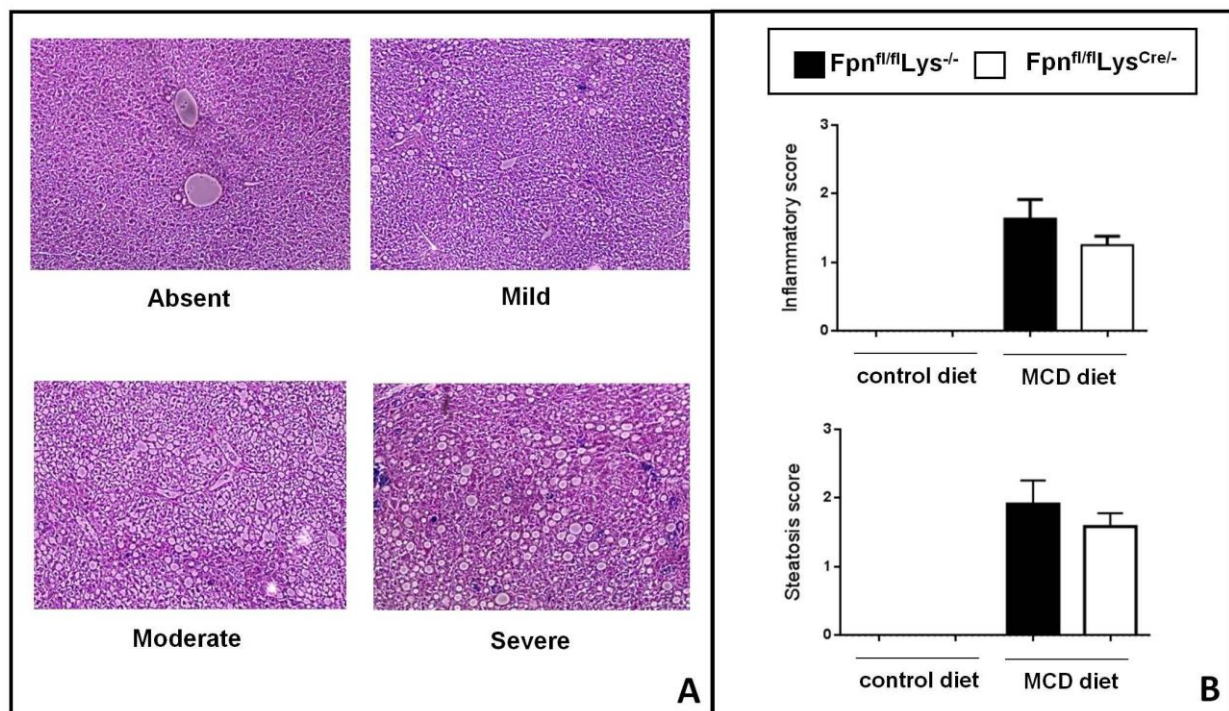
Figure 34. Steatohepatitis induced by MCD diet is not affected by Fpn deletion in macrophages in Fpn$^{fl/fl}$Lys$^{Cre/-}$ mice.

A) Liver histology representative of the inflammatory and steatosis scores. Tissue sections were stained with hematoxylin and eosin staining. Magnification 10X.

B) Histological grading of hepatic inflammation and steatosis: 0 = absent; 1 = mild; 2 = moderate; 3 = severe. Data are presented as mean ± SEM.

5.10 Iron retention in macrophages does not affect liver fibrosis induced by MCD diet

In the attempt to better characterize the role of macrophage iron in these settings, we evaluated the levels of cytokines with inflammatory and fibrogenic functions in mice fed the MCD diet. The expression of the pro-inflammatory mediators TNFα, IL-6 and CCL2did not show significant differences between Fpn$^{fl/fl}$Lys$^{Cre/-}$ mice and control littermates (Figure 35). These data suggest that Fpn deletion in macrophages does not affect the inflammatory response to liver damage, a result that confirms what we observed in the cutaneous wound healing model.

Similarly, no significant differences were observed in the expression of the fibrogenic cytokines TGF-β and TIMP-1 and in the levels of collagen I and αSMA (markers of activated fibroblasts and myofibroblasts respectively) (Figure 35).
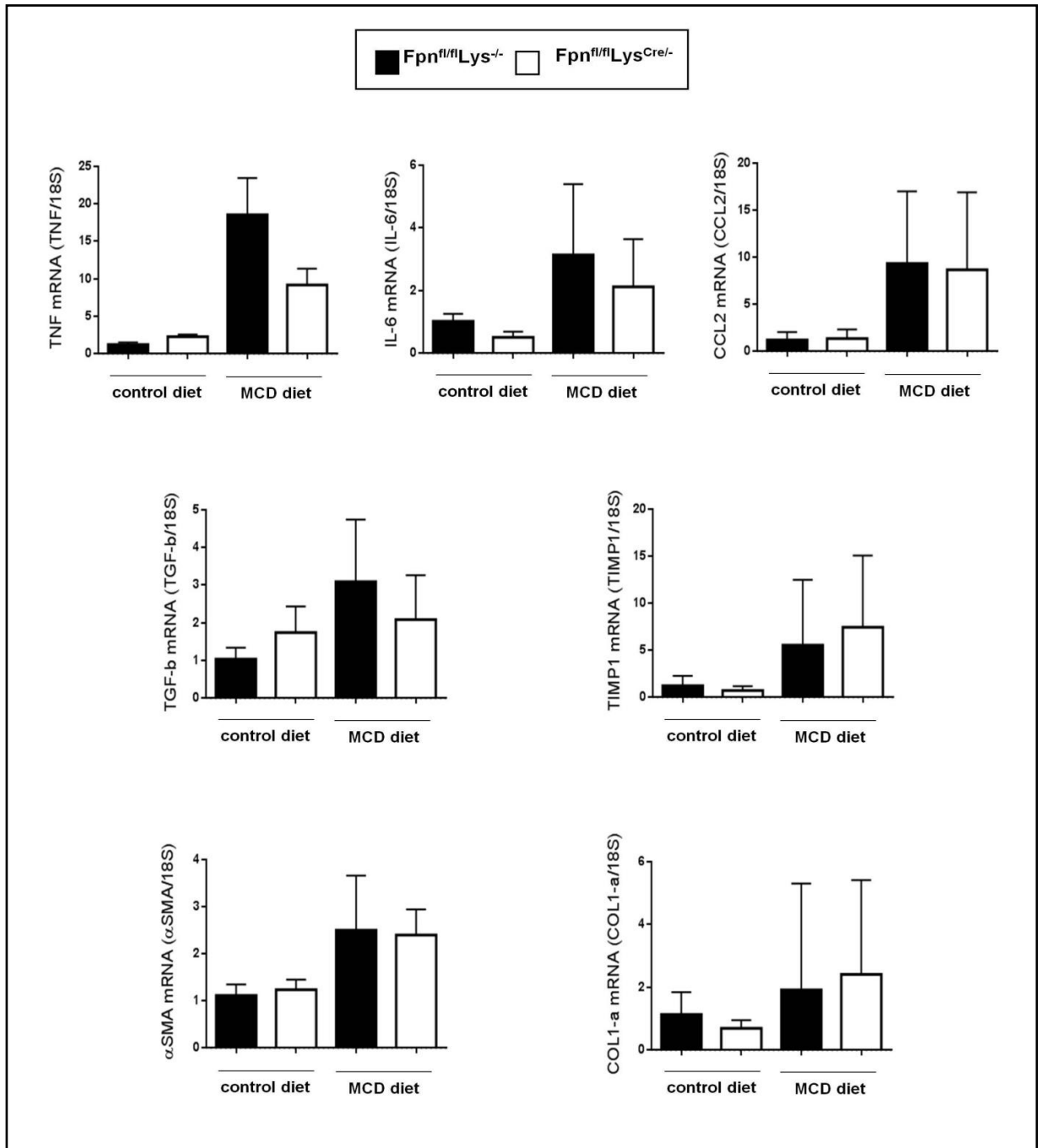
Figure 35. Inflammatory and fibrotic mediators in liver are not altered in Fpnfl/flLysCre/-mice.

TNFα, IL-6, CCL2, TGF-β, TIMP-1, αSMA and COL1-a mRNA levels in liver from Fpnfl/flLys-/- and Fpnfl/flLysCre/- mice. mRNA levels were measured by quantitative RT-PCR and normalized to the housekeeping gene 18S RNA (mean ± SEM of n = 10 mice for each group; ** p < 0.001).

Histological analysis of liver sections using Sirius red staining to assess collagen deposition (Figure 36A) gave similar results: animals exposed to the control diet had no sign of fibrosis, while mice fed on MCD diet showed mild to moderate perisinusoidal fibrosis, but without significant differences between Fpn^{fl/fl}Lys^{Cre/-} mice and control littermates. The results were confirmed by a blinded evaluation (Figure 36B).
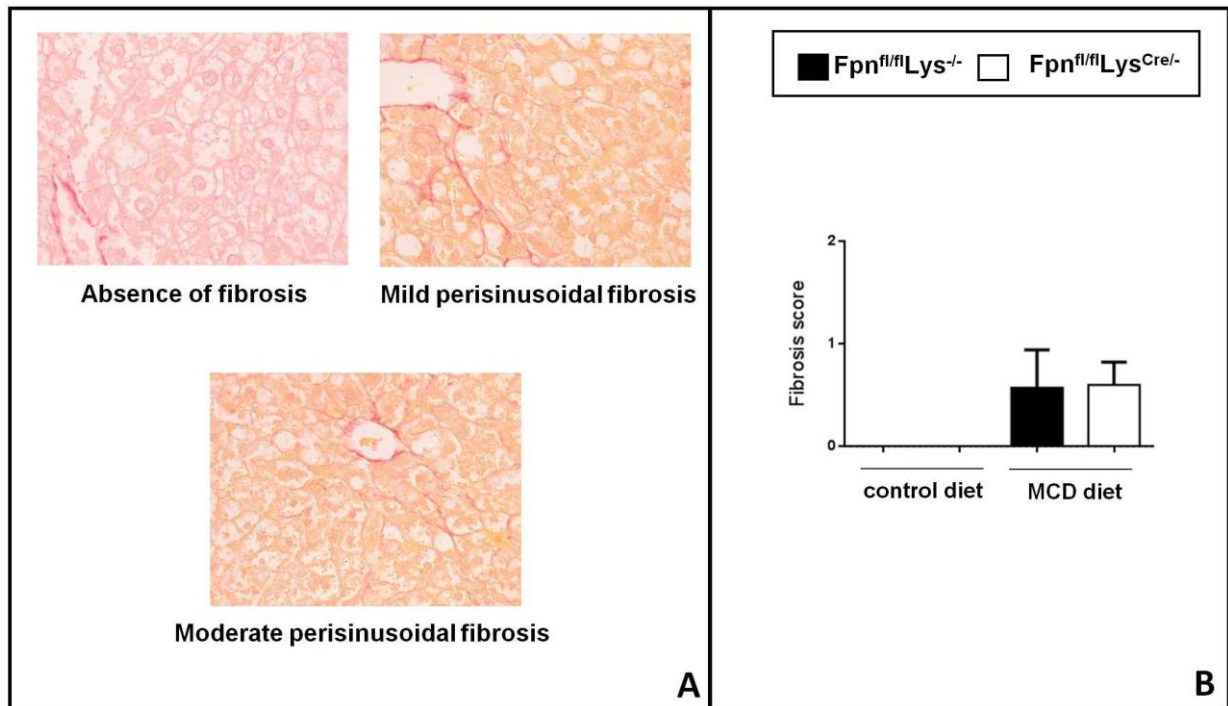
Figure 36. Fibrosis induced by MCD diet is not affected by Fpn deletion in macrophages in Fpn$^{fl/fl}$Lys$^{Cre/-}$mice.

A) Liver histology representative of the fibrosis scores. Tissue sections were stained with Sirius red staining. Magnification 10X.

B) Histological grading of hepatic fibrosis: 0 = absence of fibrosis; 1 = mild perisinusoidal fibrosis; 2 = moderate perisinusoidal fibrosis. Data are presented as mean ± SEM.

In summary, these results indicate that, in this liver injury model, there are no differences in the inflammatory response to liver damage and in fibrogenesis. The different levels of transaminases are probably due to a different susceptibility of Fpn$^{fl/fl}$Lys$^{Cre/-}$ mice to liver damage, a result that should be further investigated, maybe using another model of liver fibrosis.

6. DISCUSSION

In line with the increasing awareness that macrophages have an important trophic role in addition to their immunological function [81], the studies reported in this thesis were mainly focused on exploiting a mouse model with Fpn inactivation in macrophages to explore the role of iron release from macrophages in tissue homeostasis and regeneration. The role of macrophages of the reticuloendothelial system as a source of iron for erythroid progenitor cells is well established [82], but we hypothesized for macrophages a role as "local iron redistributors" in other tissues, where macrophages manage iron availability for neighbouring cells.

Since iron metabolism can be quite different among various mouse strains [72-74], we first characterized our model in which macrophage Fpn was inactivated in C57BL/6J mice and compared the phenotype with previously published results obtained in the 129/SvEvTac background [71]. Actually, we found significant differences also in the absence of any pathological stimulus (see below). Although it is known that the efficiency of the Cre/Lox system is not complete, Fpn deletion in macrophages of Fpn^{fl/fl}Lys[Cre/-] mice was able to cause the expected iron accumulation in spleen macrophages. Other types of macrophages, such as liver Kupffer cells and BMDM, showed the same increase in iron deposition. Iron retention was accompanied by a significant decrease in serum iron and hence by lower Hb levels and Htc at3 weeks after birth. However, all blood parameters rapidly returned to normal levels after weaning and remained almost unaltered until 18 weeks, indicating a compensatory effect by increased absorption of dietary iron.

Notably, Fpn^{fl/fl}Lys[Cre/-] mice showed diffuse alopecia at birth without the involvement of the head. This phenotype has not been reported in mice lacking macrophage Fpn maintained on the 129/SvEvTac background,

thus reinforcing the concept that some aspects of iron homeostasis are strain-specific. In the attempt to better characterize this condition, we observed a moderate to severe coalescing dilatation of hair follicles, which contain remnants of hair shafts and keratin, and slight achantosis of the superficial epidermis. Hair started to regrow 2 weeks after weaning and was full regrown at four weeks of age. Histological analysis showed that minor skin alterations were still detectable in adult mice with normal hair. These observations indicating that Fpn deletion in macrophages causes severe alterations of the hair follicle and epidermis are in line with similar hair and skin lesions observed in mice with altered expression of other proteins of iron metabolism [83-85] and indicate the key role of iron in these settings, though in the above mentioned studies the presence of systemic iron deficiency did not allow the authors to distinguish the effect of low systemic iron levels from the actual local availability of macrophage-derived iron. To better understand if alopecia in our mice was a consequence of systemic iron deficiency or a local effect of iron sequestration in macrophages, we determined the effect of an iron-restricted diet on hair growth of both mice populations. During induction of iron-deficiency both $Fpn^{fl/fl}Lys^{Cre/-}$ and control littermates suffered of iron-dependent anemia, but only mice with loss of macrophage Fpn were affected by alopecia, whereas control mice, no matter how long they were fed the low iron diet, never lost hair. Furthermore, no relevant gross and histopathological changes were found in the dorsal haired skin of control mice maintained in prolonged iron deficiency. Accordingly, after the reintroduction of a normal diet, serum iron, Hb and Hct of $Fpn^{fl/fl}Lys^{Cre/-}$ mice returned to normal levels 2 weeks before the restoration of normally haired skin, thus confirming that alopecia and hypoferremia/anemia are not directly associated. These results raised the

question of which functions can be compromised by iron scarcity in epidermal cells. In keeping with previous results showing that iron released via Fpn from human in vitro differentiated macrophages supports in vitro cell proliferation [29], an important role for the numerous skin macrophages could be the release of sufficient iron for the multiplication of growing cells in the microenvironment. In fact, the expression of the proliferation marker Ki67 was significantly decreased in fast growing epithelial cells of the hair bulbs of 3-week-old Fpn$^{fl/fl}$Lys$^{Cre/-}$ mice, compared to controls. The demonstration that TfR1 expression, indicative of low iron levels, is increased in the same epithelial follicle cells if tissue macrophage lack Fpn, supports the conclusion that Fpn-dependent iron release from macrophages is essential for correct tissue homeostasis, in particular to sustain the rapid growth of hair follicle cells. Notably, a recent study has shown that macrophages are part of the stem cell niche in various tissues [86] and the results reported here raise the possibility that macrophage dependent iron metabolism could have a specific role in stem cell niches.

These conclusions were confirmed by our data obtained using a cutaneous wound healing model, a prototypic situation of tissue repair in which macrophages play a key role [38]. In line with the importance of macrophage iron release for tissue homeostasis, we observed in Fpn$^{fl/fl}$Lys$^{Cre/-}$ mice a considerable delay in the process of wound healing, with a lag of 3-5 days in the wound closure and delayed granulation tissue formation. Given the role of macrophages in the development of inflammation, it was important to establish whether the defective wound healing observed in Fpn$^{fl/fl}$Lys$^{Cre/-}$ mice was the result of an altered inflammatory response. Analysis of macrophage production of inflammatory molecules, of content of different leukocyte subsets and of

macrophages polarization capability showed no differences in Fpn$^{fl/fl}$Lys$^{Cre/-}$ mice compared to controls, indicating that the delay in the process of wound closure that we observed is not a consequence of a different inflammatory response. To date, the role of iron in macrophage activity during inflammation is unclear: an increased inflammatory response was found in iron-depleted macrophages [87], but not in equally iron-deficient macrophages from HFE$^{-/-}$ mice model [88]. Other studies showed that iron chelation reduced the synthesis of proinflammatory cytokines in isolated macrophages [89], whereas TNFα and IL-6 production were increased in Fpn-deficient macrophages with iron accumulation[71]. These contradictory results may be related to the different experimental models, the heterogeneity of macrophages, the exposure to different sources of iron and stimuli, etc. In our model, iron accumulation in macrophages did not aggravate the inflammatory response in wound healing, a finding in line with a recent study showing that iron did not increase M1 polarization of RAW264.7 macrophages [90].

We then hypothesized that the disruption of iron export from macrophages due to Fpn deficiency could delay wound healing by preventing nearby mesenchymal and stromal cells from receiving adequate iron supply for proper proliferation and differentiation. In line with the higher Fpn expression in M2 macrophages compared to M1 [29,32], the lack of macrophage Fpn should exert its major effects in the late phase of repair. Indeed, in the late stages, normal M2 macrophages export iron through enhanced Fpn expression, whereas Fpn$^{fl/fl}$Lys$^{Cre/-}$ mice macrophages accumulate iron with concomitant induction of Ft and repression of TfR1 expression. In fact, the lower fibrosis score and the decreased expression of collagen-1, αSMA and PDGFRa showed that in Fpn$^{fl/fl}$Lys$^{Cre/-}$ mice the stromal component is compromised. Moreover,

our results show that macrophage iron is also essential for the development of both lymphatic and blood vascular network in face of unchanged levels of angiogenic and fibrogenic factors like VEGF and TGF-β. Finally, loss of macrophage Fpn impaired cell proliferation, as shown by decreased Ki67 expression. Taken together, these results indicate that, though it does not interfere with immune cells recruitment and local activation, Fpn deletion in macrophages impairs blood vessels formation and stromal cells proliferation, leading to delayed skin repair. In summary, we showed that the correct Fpn-iron supply from macrophages is essential for tissue homeostasis both in physiological and pathological conditions in a tissue, the skin characterized by a fast cell growth [91].

Given the results we obtained from cutaneous wound healing, we decided to explore another useful model of tissue repair: liver fibrosis, a process in which macrophages play a key role [54,55]. To investigate how macrophage derived iron could influence this process, we used the MCD diet model, which causes a liver injury similar to that occurring in human NAFDL. The first results obtained in animals exposed to the MCD diet showed that the levels of both ALT and AST in Fpn$^{fl/fl}$Lys$^{Cre/-}$ were significantly lower compared to controls, indicating a less severe cell damage. Then, we tried to investigate the possible consequences of this difference by evaluating inflammation and steatosis. However, no significant differences between Fpn$^{fl/fl}$Lys$^{Cre/-}$ mice and control mice exposed to the same diet were found when we analysed liver histology and measured the expression of various inflammatory cytokines, although a trend toward lower levels of TNFα and IL-6 mRNA was evident. These data suggested that Fpn deletion in macrophages does not affect the inflammatory response to liver damage, confirming the results in the

cutaneous wound healing. We then decided to explore the effect of Fpn deletion in macrophages on stromal cells and ECM deposition by analysing specifically the fibrosis process. No significant differences were observed in the expression of the fibrogenic cytokines TGF-β and TIMP-1 and in the levels of collagen I and αSMA. Moreover, staining of liver sections for collagen confirmed the lack of statistically significant differences in fibrosis score between Fpn$^{fl/fl}$Lys$^{Cre/-}$ mice and controls. In summary, these preliminary results show no differences either in the inflammatory response nor in the activity of stromal cells between Fpn$^{fl/fl}$Lys$^{Cre/-}$ mice and controls. The only significant difference, represented by transaminases levels, is probably attributable to a resistance of our model to hepatic injury, rather than an altered inflammatory/fibrotic response.

In conclusion, the different results we observed in the two models should be further investigated, to better elucidate the diversity between the effect of iron retention in macrophages in the cutaneous wound healing and in the process of hepatic fibrosis. Particularly, the cause of the hypothetical resistance of our model to liver damage should be explored. In this respect, in addition to performing other experiments with the MCD diet model, we are considering to use another model of liver fibrosis.

Despite these inconsistencies that should be further explored, it seems possible to conclude that the results reported in this thesis indicate that the macrophage trophic function in skin homeostasis and healing is iron and Fpn-dependent. Interestingly, a requirement for iron provided by macrophages similar to the one we observed in the skin has been recently described for the repair of skeletal muscle cells [92].Therefore, iron should be added to the list of trophic mediators produced by

macrophages that stimulate the growth, differentiation and activity of neighboring parenchymal and stromal cells in order to maintain tissue homeostasis or promote repair.

7. BIBLIOGRAPHY

1. Hernandez-Gea V, Friedman SL. Pathogenesis of liver fibrosis. *Annu Rev Pathol*. 2011;6:425-456.

2. Ganz T. Hepcidin and iron regulation, 10 years later. *Blood*. 2011;117(17):4425-4433.

3. Gurtner GC, Werner S, Barrandon Y, Longaker MT. Wound repair and regeneration. *Nature*. 2008;453(7193):314-321.

4. Andrews NC, Schmidt PJ. Iron homeostasis. *Annu Rev Physiol*. 2007;69:69-85.

5. Pantopoulos K, Porwal SK, Tartakoff A, Devireddy L. Mechanisms of mammalian iron homeostasis. *Biochemistry*. 2012;51(29):5705-5724.

6. Cairo G, Bernuzzi F, Recalcati S. A precious metal: Iron, an essential nutrient for all cells. *Genes Nutr*. 2006;1(1):25-39.

7. Drakesmith H, Prentice AM. Hepcidin and the iron-infection axis. *Science*. 2012;338(6108):768-772.

8. Muckenthaler MU, Rivella S, Hentze MW, Galy B. A Red Carpet for Iron Metabolism. *Cell*. 2017;168(3):344-361.

9. Haldar M, Kohyama M, So AY, et al. Heme-mediated SPI-C induction promotes monocyte differentiation into iron-recycling macrophages. *Cell*. 2014;156(6):1223-1234.

10. Ganz T. Systemic iron homeostasis. *Physiol Rev*. 2013;93(4):1721-1741.

11. Theil EC. Iron, ferritin, and nutrition. *Annu Rev Nutr*. 2004;24:327-343.

12. Donovan A, Lima CA, Pinkus JL, et al. The iron exporter ferroportin/Slc40a1 is essential for iron homeostasis. *Cell Metab*. 2005;1(3):191-200.

13. Nemeth E, Tuttle MS, Powelson J, et al. Hepcidin regulates cellular iron efflux by binding to ferroportin and inducing its internalization. *Science*. 2004;306(5704):2090-2093.

14. Nicolas G, Chauvet C, Viatte L, et al. The gene encoding the iron regulatory peptide hepcidin is regulated by anemia, hypoxia, and inflammation. *J Clin Invest*. 2002;110(7):1037-1044.

15. Nemeth E, Valore EV, Territo M, Schiller G, Lichtenstein A, Ganz T. Hepcidin, a putative mediator of anemia of inflammation, is a type II acute-phase protein. *Blood*. 2003;101(7):2461-2463.

16. Wrighting DM, Andrews NC. Interleukin-6 induces hepcidin expression through STAT3. *Blood*. 2006;108(9):3204-3209.

17. Zoller EE, Lykens JE, Terrell CE, et al. Hemophagocytosis causes a consumptive anemia of inflammation. *J Exp Med*. 2011;208(6):1203-1214.

18. Mayle KM, Le AM, Kamei DT. The intracellular trafficking pathway of transferrin. *Biochim Biophys Acta*. 2012;1820(3):264-281.

19. Daniels TR, Delgado T, Rodriguez JA, Helguera G, Penichet ML. The transferrin receptor part I: Biology and targeting with cytotoxic antibodies for the treatment of cancer. *Clin Immunol*. 2006;121(2):144-158.

20. Harrison PM, Arosio P. The ferritins: molecular properties, iron storage function and cellular regulation. *Biochim Biophys Acta*. 1996;1275(3):161-203.

21. Wallace DF, Harris JM, Subramaniam VN. Functional analysis and theoretical modeling of ferroportin reveals clustering of mutations according to phenotype. *Am J Physiol Cell Physiol*. 2010;298(1):C75-84.

22. Taniguchi R, Kato HE, Font J, et al. Outward- and inward-facing structures of a putative bacterial transition-metal transporter with homology to ferroportin. *Nat Commun*. 2015;6:8545.

23. Taylor M, Qu A, Anderson ER, et al. Hypoxia-inducible factor-2a mediates the adaptive increase of intestinal ferroportin during iron deficiency in mice. *Gastroenterology*. 2011;140(7):2044-2055.

24. Deschemin JC, Vaulont S. Role of hepcidin in the setting of hypoferremia during acute inflammation. *PLoS One*. 2013;8(4):e61050.

25. Guida C, Altamura S, Klein FA, et al. A novel inflammatory pathway mediating rapid hepcidin-independent hypoferremia. *Blood*. 2015;125(14):2265-2275.

26. Lymboussaki A, Pignatti E, Montosi G, Garuti C, Haile DJ, Pietrangelo A. The role of the iron responsive element in the control of ferroportin1/IREG1/MTP1 gene expression. *J Hepatol*. 2003;39(5):710-715.

27. Qiao B, Sugianto P, Fung E, et al. Hepcidin-induced endocytosis of ferroportin is dependent on ferroportin ubiquitination. *Cell Metab*. 2012;15(6):918-924.

28. Gordon S, Martinez FO. Alternative activation of macrophages: mechanism and functions. *Immunity*. 2010;32(5):593-604.

29. Recalcati S, Locati M, Marini A, et al. Differential regulation of iron homeostasis during human macrophage polarized activation. *Eur J Immunol*. 2010;40(3):824-835.

30. Cairo G, Recalcati S, Mantovani A, Locati M. Iron trafficking and metabolism in macrophages: contribution to the polarized phenotype. *Trends Immunol*. 2011;32(6):241-247.

31. Sica A, Mantovani A. Macrophage plasticity and polarization: in vivo veritas. *J Clin Invest*. 2012;122(3):787-795.

32. Corna G, Campana L, Pignatti E, et al. Polarization dictates iron handling by inflammatory and alternatively activated macrophages. *Haematologica*. 2010;95(11):1814-1822.

33. Vallelian F, Schaer CA, Kaempfer T, et al. Glucocorticoid treatment skews human monocyte differentiation into a hemoglobin-clearance phenotype with enhanced heme-iron recycling and antioxidant capacity. *Blood*. 2010;116(24):5347-5356.

34. Prasse A, Pechkovsky DV, Toews GB, et al. A vicious circle of alveolar macrophages and fibroblasts perpetuates pulmonary fibrosis via CCL18. *Am J Respir Crit Care Med*. 2006;173(7):781-792.

35. Mora AL, Torres-González E, Rojas M, et al. Activation of alveolar macrophages via the alternative pathway in herpesvirus-induced lung fibrosis. *Am J Respir Cell Mol Biol*. 2006;35(4):466-473.

36. Kato GJ. Haptoglobin halts hemoglobin's havoc. *J Clin Invest*. 2009;119(8):2140-2142.

37. Brancato SK, Albina JE. Wound macrophages as key regulators of repair: origin, phenotype, and function. *Am J Pathol*. 2011;178(1):19-25.

38. Wynn TA, Vannella KM. Macrophages in Tissue Repair, Regeneration, and Fibrosis. *Immunity*. 2016;44(3):450-462.

39. Mantovani A, Biswas SK, Galdiero MR, Sica A, Locati M. Macrophage plasticity and polarization in tissue repair and remodelling. *J Pathol*. 2013;229(2):176-185.

40. Stenn KS, Paus R. Controls of hair follicle cycling. *Physiol Rev*. 2001;81(1):449-494.

41. Castellana D, Paus R, Perez-Moreno M. Macrophages contribute to the cyclic activation of adult hair follicle stem cells. *PLoS Biol*. 2014;12(12):e1002002.

42. Mirza R, DiPietro LA, Koh TJ. Selective and specific macrophage ablation is detrimental to wound healing in mice. *Am J Pathol*. 2009;175(6):2454-2462.

43. Singer AJ, Clark RA. Cutaneous wound healing. *N Engl J Med*. 1999;341(10):738-746.

44. Schultz GS, Davidson JM, Kirsner RS, Bornstein P, Herman IM. Dynamic reciprocity in the wound microenvironment. *Wound Repair Regen*. 2011;19(2):134-148.

45. Mahdavian Delavary B, van der Veer WM, van Egmond M, Niessen FB, Beelen RH. Macrophages in skin injury and repair. *Immunobiology*. 2011;216(7):753-762.

46. Clark RAF. Wound Repair. In: Clark RAF, ed. The Molecular and Cellular Biology of Wound Repair. Boston, MA: Springer US; 1988:3-50.

47. Leask A, Abraham DJ. TGF-beta signaling and the fibrotic response. *FASEB J*. 2004;18(7):816-827.

48. Lucas T, Waisman A, Ranjan R, et al. Differential roles of macrophages in diverse phases of skin repair. *J Immunol*. 2010;184(7):3964-3977.

49. Darby I, Skalli O, Gabbiani G. Alpha-smooth muscle actin is transiently expressed by myofibroblasts during experimental wound healing. *Lab Invest*. 1990;63(1):21-29.

50. Hinz B. Formation and function of the myofibroblast during tissue repair. *J Invest Dermatol*. 2007;127(3):526-537.

51. Sindrilaru A, Peters T, Wieschalka S, et al. An unrestrained proinflammatory M1 macrophage population induced by iron impairs wound healing in humans and mice. *J Clin Invest*. 2011;121(3):985-997.

52. Markolovic S, Wilkins SE, Schofield CJ. Protein Hydroxylation Catalyzed by 2-Oxoglutarate-dependent Oxygenases. *J Biol Chem*. 2015;290(34):20712-20722.

53. Chalasani N, Younossi Z, Lavine JE, et al. The diagnosis and management of non-alcoholic fatty liver disease: practice Guideline by the American Association for the Study of Liver Diseases, American College of Gastroenterology, and the American Gastroenterological Association. *Hepatology*. 2012;55(6):2005-2023.

54. Wynn TA, Barron L. Macrophages: master regulators of inflammation and fibrosis. *Semin Liver Dis*. 2010;30(3):245-257.

55. Ramachandran P, Iredale JP. Macrophages: central regulators of hepatic fibrogenesis and fibrosis resolution. *J Hepatol*. 2012;56(6):1417-1419.

56. Duffield JS, Lupher M, Thannickal VJ, Wynn TA. Host responses in tissue repair and fibrosis. *Annu Rev Pathol*. 2013;8:241-276.

57. Browning JD, Horton JD. Molecular mediators of hepatic steatosis and liver injury. *J Clin Invest*. 2004;114(2):147-152.

58. Itagaki H, Shimizu K, Morikawa S, Ogawa K, Ezaki T. Morphological and functional characterization of non-alcoholic fatty liver disease induced by a methionine-choline-deficient diet in C57BL/6 mice. *Int J Clin Exp Pathol*. 2013;6(12):2683-2696.

59. Sica A, Invernizzi P, Mantovani A. Macrophage plasticity and polarization in liver homeostasis and pathology. *Hepatology*. 2014;59(5):2034-2042.

60. Barron L, Wynn TA. Fibrosis is regulated by Th2 and Th17 responses and by dynamic interactions between fibroblasts and macrophages. *Am J Physiol Gastrointest Liver Physiol*. 2011;300(5):G723-728.

61. Pietrangelo A. Iron-induced oxidant stress in alcoholic liver fibrogenesis. *Alcohol*. 2003;30(2):121-129.

62. Valenti L, Dongiovanni P, Fracanzani AL, Fargion S. HFE mutations in nonalcoholic fatty liver disease. *Hepatology*. 2008;47(5):1794-1795; author reply 1795-1796.

63. Recalcati S, Locati M, Cairo G. Systemic and cellular consequences of macrophage control of iron metabolism. *Semin Immunol*. 2012;24(6):393-398.

64. Pietrangelo A. Iron, oxidative stress and liver fibrogenesis. *J Hepatol*. 1998;28 Suppl 1:8-13.

65. Valenti L, Dongiovanni P, Piperno A, et al. Alpha 1-antitrypsin mutations in NAFLD: high prevalence and association with altered iron metabolism but not with liver damage. *Hepatology*. 2006;44(4):857-864.

66. Valenti L, Fracanzani AL, Bugianesi E, et al. HFE genotype, parenchymal iron accumulation, and liver fibrosis in patients with nonalcoholic fatty liver disease. *Gastroenterology*. 2010;138(3):905-912.

67. Nakayama Y, Kon S, Kurotaki D, Morimoto J, Matsui Y, Uede T. Blockade of interaction of alpha9 integrin with its ligands hinders the formation of granulation in cutaneous wound healing. *Lab Invest*. 2010;90(6):881-894.

68. Weischenfeldt J, Porse B. Bone Marrow-Derived Macrophages (BMM): Isolation and Applications. *CSH Protoc*. 2008;2008:pdb.prot5080.

69. Zhang X, Goncalves R, Mosser DM. The isolation and characterization of murine macrophages. *Curr Protoc Immunol*. 2008;Chapter 14:Unit 14.11.

70. Delaby C, Pilard N, Gonçalves AS, Beaumont C, Canonne-Hergaux F. Presence of the iron exporter ferroportin at the plasma

membrane of macrophages is enhanced by iron loading and down-regulated by hepcidin. *Blood*. 2005;106(12):3979-3984.

71. Zhang Z, Zhang F, An P, et al. Ferroportin1 deficiency in mouse macrophages impairs iron homeostasis and inflammatory responses. *Blood*. 2011;118(7):1912-1922.

72. Leboeuf RC, Tolson D, Heinecke JW. Dissociation between tissue iron concentrations and transferrin saturation among inbred mouse strains. *J Lab Clin Med*. 1995;126(2):128-136.

73. Morse AC, Beard JL, Jones BC. A genetic developmental model of iron deficiency: biological aspects. *Proc Soc Exp Biol Med*. 1999;220(3):147-152.

74. Clothier B, Robinson S, Akhtar RA, et al. Genetic variation of basal iron status, ferritin and iron regulatory protein in mice: potential for modulation of oxidative stress. *Biochem Pharmacol*. 2000;59(2):115-122.

75. Kautz L, Jung G, Valore EV, Rivella S, Nemeth E, Ganz T. Identification of erythroferrone as an erythroid regulator of iron metabolism. *Nat Genet*. 2014;46(7):678-684.

76. Kroner A, Greenhalgh AD, Zarruk JG, Passos Dos Santos R, Gaestel M, David S. TNF and increased intracellular iron alter macrophage polarization to a detrimental M1 phenotype in the injured spinal cord. *Neuron*. 2014;83(5):1098-1116.

77. Vinchi F, Costa da Silva M, Ingoglia G, et al. Hemopexin therapy reverts heme-induced proinflammatory phenotypic switching of macrophages in a mouse model of sickle cell disease. *Blood*. 2016;127(4):473-486.

78. Pickens MK, Yan JS, Ng RK, et al. Dietary sucrose is essential to the development of liver injury in the methionine-choline-deficient model of steatohepatitis. *J Lipid Res*. 2009;50(10):2072-2082.

79. Yao ZM, Vance DE. The active synthesis of phosphatidylcholine is required for very low density lipoprotein secretion from rat hepatocytes. *J Biol Chem*. 1988;263(6):2998-3004.

80. Caballero F, Fernández A, Matías N, et al. Specific contribution of methionine and choline in nutritional nonalcoholic steatohepatitis:

impact on mitochondrial S-adenosyl-L-methionine and glutathione. *J Biol Chem*. 2010;285(24):18528-18536.

81. Wynn TA, Chawla A, Pollard JW. Macrophage biology in development, homeostasis and disease. *Nature*. 2013;496(7446):445-455.

82. Drakesmith H, Nemeth E, Ganz T. Ironing out Ferroportin. *Cell Metab*. 2015;22(5):777-787.

83. Nicolas G, Bennoun M, Porteu A, et al. Severe iron deficiency anemia in transgenic mice expressing liver hepcidin. *Proc Natl Acad Sci U S A*. 2002;99(7):4596-4601.

84. Du X, She E, Gelbart T, et al. The serine protease TMPRSS6 is required to sense iron deficiency. *Science*. 2008;320(5879):1088-1092.

85. Folgueras AR, de Lara FM, Pendás AM, et al. Membrane-bound serine protease matriptase-2 (Tmprss6) is an essential regulator of iron homeostasis. *Blood*. 2008;112(6):2539-2545.

86. Kaur S, Raggatt LJ, Batoon L, Hume DA, Levesque JP, Pettit AR. Role of bone marrow macrophages in controlling homeostasis and repair in bone and bone marrow niches. *Semin Cell Dev Biol*. 2017;61:12-21.

87. Pagani A, Nai A, Corna G, et al. Low hepcidin accounts for the proinflammatory status associated with iron deficiency. *Blood*. 2011;118(3):736-746.

88. Roy CN, Custodio AO, de Graaf J, et al. An Hfe-dependent pathway mediates hyposideremia in response to lipopolysaccharide-induced inflammation in mice. *Nat Genet*. 2004;36(5):481-485.

89. Wang L, Johnson EE, Shi HN, Walker WA, Wessling-Resnick M, Cherayil BJ. Attenuated inflammatory responses in hemochromatosis reveal a role for iron in the regulation of macrophage cytokine translation. *J Immunol*. 2008;181(4):2723-2731.

90. Gan ZS, Wang QQ, Li JH, Wang XL, Wang YZ, Du HH. Iron Reduces M1 Macrophage Polarization in RAW264.7 Macrophages

Associated with Inhibition of STAT1. *Mediators Inflamm.* 2017;2017:8570818.

91.   Ansell DM, Kloepper JE, Thomason HA, Paus R, Hardman MJ. Exploring the "hair growth-wound healing connection": anagen phase promotes wound re-epithelialization. *J Invest Dermatol.* 2011;131(2):518-528.

92.   Corna G, Caserta I, Monno A, et al. The Repair of Skeletal Muscle Requires Iron Recycling through Macrophage Ferroportin. *J Immunol.* 2016;197(5):1914-1925.